Medical Image Computing at CSE-Yonsei

Jin Keun Seo

Computational Science & Engineering
Yonsei University, Korea

KAIST Medical Imaging Seminar (2014.7.30)

Electrical/Mechanical Tissue Property Imaging

Due to nutritional and metabolic disorder, the physical property of a biological tissue will change according to the change in tissue composition.

- **Electrical Property (0 Hz $\leq \omega/2\pi \leq$ 1MHz):**

$$\nabla \cdot ((\sigma + i\omega\epsilon)\nabla u) = 0$$

- **Electrical Property (100kHz$\leq \omega/2\pi \leq$ 1GHz):**

$$-\nabla^2 \mathbf{H} = \frac{\nabla(\sigma + i\omega\epsilon)}{\sigma + i\omega\epsilon} \times \nabla \times \mathbf{H} - i\mu_0\omega\kappa\mathbf{H}$$

- **Mechanical Property (0 Hz $\leq \omega/2\pi \leq$ 10kHz)**

$$\nabla \cdot (\mu \nabla \mathbf{u}) + \nabla((\lambda + \mu)\nabla \cdot \mathbf{u}) = -\rho\omega^2 \mathbf{u}$$

Elliptic PDE Beginning.

Admittivity $\sigma + i\omega\epsilon$ & potential u ($\omega/2\pi \leq$ 100kHz) are connected by

$$\nabla \cdot (\underbrace{(\sigma + i\omega\epsilon)}_{3\times 3\text{matrix}} \nabla u\ ) = 0$$

- **$\sigma + i\omega\epsilon$ can be viewed as an ensemble average of pointwise admittivity (via homogenization).**
- **The effective $\sigma + i\omega\epsilon$ depends on scale and ω.**
- Math. model is derived by a suitable arrangement of Maxwell's equations: σ=conductivity, ϵ=permittivity.

Name	Time-varying Field	Time-harmonic Field
Gauss's law	$\nabla \cdot \mathbf{B} = 0$	$\nabla \cdot \mathbf{B} = 0$
Faraday's law	$\nabla \times \mathbf{E} = -\frac{\partial}{\partial t}\mathbf{B}$	$\nabla \times \mathbf{E} = -\mathrm{i}\omega\mathbf{B}$
Ampére's law	$\nabla \times \mathbf{H} = \sigma\mathbf{E} + \frac{\partial}{\partial t}\mathbf{D}$	$\nabla \times \mathbf{H} = (\sigma + \mathrm{i}\omega\epsilon)\mathbf{E}$

What type of effective $\kappa = \sigma + i\omega\epsilon$ can you visualize?

$$\nabla \cdot ((\sigma + i\omega\epsilon)\ \nabla u\ ) = 0$$

- The effective admittivity spectra should be useful as a means of **assessing disease process**.
- **Robust reconstruction** $\leftrightarrow$ **Measurable quantities** with taking account of well-posedness (existence, uniqueness, stability) of the inverse model.
- Want to observe **anisotropy of tissue decreasing with** ω.

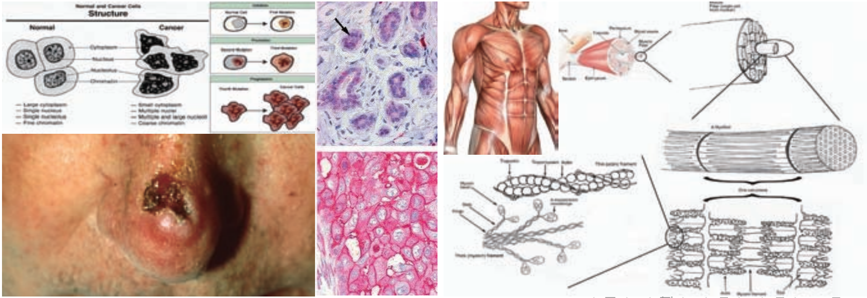

Conductivity σ describes material's ability to transport charge.

✓ $\sigma \quad \propto \quad t_{\mathsf{CA}}$: **characteristic time average of the charge particle.**

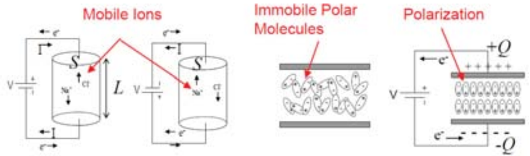

- $\mathbf{J}$ is defined by considering movements of each charged particles (such as ions) inside the body due to $\mathbf{E}$.
- If its movement is **NOT** impeded by the molecular environment,

$$\mathbf{v}(t) = \frac{q}{m}\, t\, \mathbf{E} \nearrow \infty \quad \left(\text{ from } \quad q\mathbf{E} = \text{mass } \frac{d}{dt}\mathbf{v}\right)$$

- However, its movement is **impeded by its molecular environment** so that the particle's average drift velocity $\langle \mathbf{v} \rangle_{ave}$ can be determined by the molecular structure:

$$\langle \mathbf{v} \rangle_{ave} = \frac{q}{m}\, t_{\mathsf{CA}}\, \mathbf{E} \qquad \left(\mathbf{J} = \rho \langle \mathbf{v} \rangle_{ave} \rightsquigarrow \ \sigma = \rho \frac{q}{m} t_{\mathsf{CA}}\right)$$

✓ **The permittivity ϵ is a material property determined by the polarization of the dielectric under an external electric field $\mathbf{E}$.**

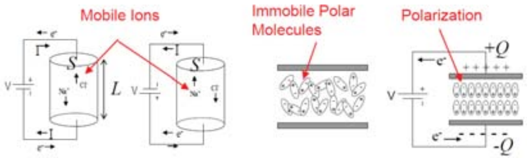

- When a dipole $\mathbf{p} := q(\mathbf{r}_\ominus - \mathbf{r}_\oplus)$ is placed in an external electric field $\mathbf{E}$, the dipole moment $\mathbf{p}$ in $\mathbf{E}$ experiences **torque**:

$$\boldsymbol{\tau} = \mathbf{r}_\oplus \times (q\mathbf{E}) + \mathbf{r}_\ominus \times (-q\mathbf{E}) = \mathbf{p} \times \mathbf{E}.$$

- The torque tends to rotate the dipole $\mathbf{p}$ to line up with $\mathbf{E}$. For non-polar molecules, $\mathbf{E}$ produces induced dipole moments by distorting the charge distributions.

$\kappa = \sigma + i\omega\epsilon$ is defined by Ohm's law:

$$\mathbf{J} = -(\sigma + i\omega\epsilon)\mathbf{E} \;\approx\; -\kappa\nabla u \qquad\qquad (\kappa = \sigma + i\omega\epsilon)$$

What type of the admittivity κ can you visualize?

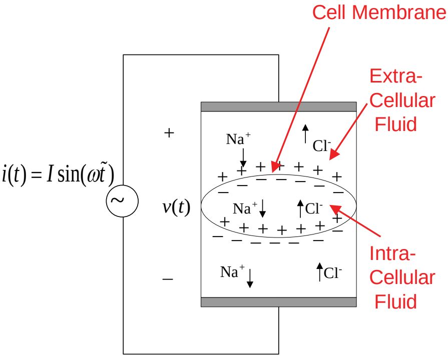

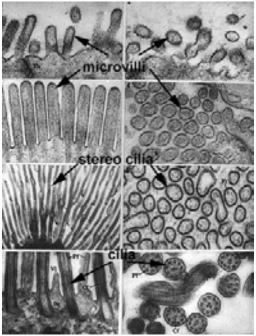

Effective conductivities of fibrous tissues are anisotropic. **What sense?**

Four different definitions of admittivity κ.

- **Pointwise admittivity** $(\kappa_{pt} = \sigma_{pt} + i\omega\epsilon_{pt})$ refers to as electrical properties at **microscopic scale.**
- **Effective admittivity** $(\kappa_{eff} = \sigma_{eff} + i\omega\epsilon_{eff})$ is defined at **macroscopic scale**. It is used to describe the **linear relationship between the ensemble mean current density and the ensemble mean electrical field**.
- **Apparent admittivity** is defined as the admittivity of locally homogeneous and isotropic medium that could yield the potential measured on the heterogeneous subject using the same applied current and arrangement of the electrodes.
- Two expressions that have the **same effective admittivity** are called **equivalent admittivity**.

What is the definition of effective admittivity ($\kappa_{eff} = \sigma_{eff} + i\omega\epsilon_{eff}$) ?

- Effective admittivity κ_{eff} in a voxel $\square$ can be viewed as

$$\int_{\square} \kappa_{\text{pt}} \nabla u_{\text{pt}} \;=\; \kappa_{\text{eff}} \int_{\square} \nabla u_{\text{pt}}$$

  for all possible potential u_{pt} satisfying $\nabla \cdot (\kappa_{\text{pt}} \nabla u_{\text{pt}}) = 0$ in a region including $\square$.

- Unfortunately, there is no such a 3×3 matrix κ_{eff} satisfying the above identity exactly in general. The best we can do is to find the optimal tensor κ_{eff} minimizing the difference......

Conductivity image   16 Channel EIT

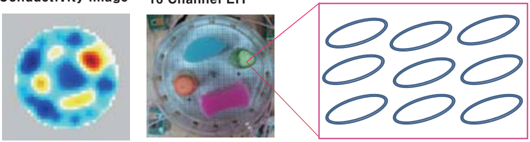

Pointwise conductivity vs Effective conductivity

- σ_{pt} and ϵ_{pt} are assumed to be isotropic and independent to ω.
- σ_{eff} and ϵ_{eff} can be approximately represented by 3×3 symmetric matrix.
- **σ_{eff} and ϵ_{eff} depend on the frequency ω.**

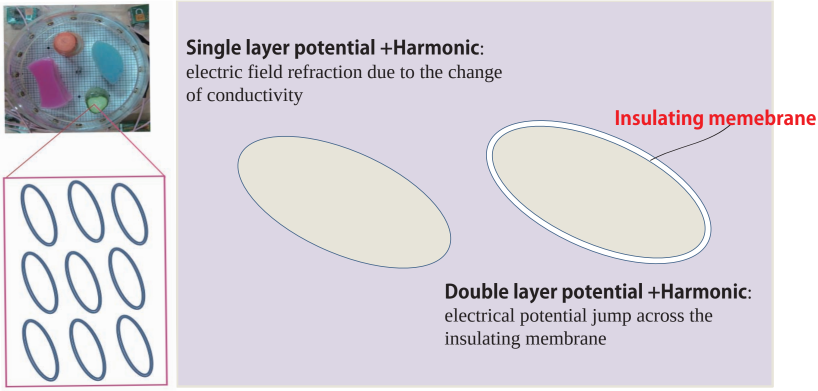

σ_{eff} and ϵ_{eff} of biological tissue depend on the frequency ω.

✓ For biological subject such as carrot and cucumber, $\frac{\partial}{\partial\omega}\sigma_{eff} \not\approx 0$ and $\frac{\partial}{\partial\omega}\epsilon_{eff} \not\approx 0$ due to the presence of membrane.

✓ For non-biological subject, $\frac{\partial}{\partial\omega}\sigma_{eff} \approx 0$ and $\frac{\partial}{\partial\omega}\epsilon_{eff} \approx 0$ due to the absence of membranes.

· Measuring frequency dependent behavior of effective conductivity increases distinguishability.

16 Channel EIT

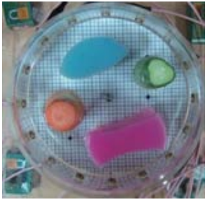

10kHz

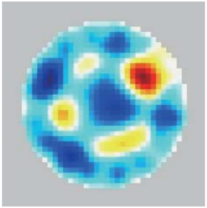

100kHz −1kHz

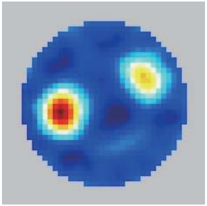

Conductivity images: (middle) tdEIT (left) fdEIT.

Homogenization (Ammari, Garnier, Giovangigli, Jing, Seo, 2013)

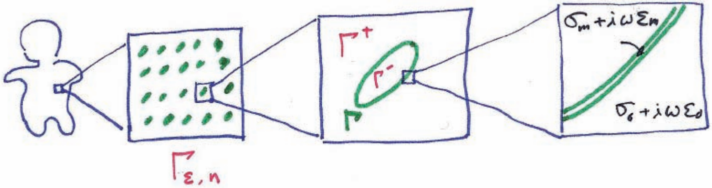

- Consider a periodic array of membranes $\Gamma_{\varepsilon,n}$ in 2D domain.
- Denoting $\kappa_m = \sigma_m + i\omega\epsilon_m$ on Γ, $\kappa_0 = \sigma_0 + i\omega\epsilon_0$ in $\Gamma^+ \cup \Gamma^-$, $\boldsymbol{\upsilon} = \frac{|\boldsymbol{\Gamma}^-|}{|\boldsymbol{\Gamma}^+ \cup \boldsymbol{\Gamma}^-|}$,

$$\nabla \cdot (\kappa_0^\omega \nabla u_\varepsilon) = 0 \text{ in } \Omega \setminus \cup_n \Gamma_{\varepsilon,n}$$
$$\left[\frac{\partial u_\varepsilon^+}{\partial n}\right] = 0 \quad \text{on} \quad \cup_n \Gamma_{\varepsilon,n}$$
$$[u_\varepsilon] - \frac{d\kappa_0^\omega}{\kappa_m^\omega} \frac{\partial u_\varepsilon}{\partial \mathbf{n}} = 0 \quad \text{on} \quad \cup_n \Gamma_{\varepsilon,n},$$

$$u_\varepsilon(\mathbf{x}) := u_0(\mathbf{x}) + u_1(\mathbf{x}, \tfrac{\mathbf{x}}{\varepsilon}) + o(\varepsilon)$$
$$u_\varepsilon \rightrightarrows u_0$$
$$\nabla u_\varepsilon \rightrightarrows \nabla u_0 + \chi_{\Gamma^-} \nabla_{\mathbf{y}} u_1 + \chi_{\Gamma^-} \nabla_{\mathbf{y}} u_1$$
$$u_1(\mathbf{x}, \mathbf{y}) = \sum_i \frac{\partial u_0}{\partial x_i}(\mathbf{x}) w_i(\mathbf{y})$$
$$\nabla \cdot ((\sigma_{eff} + i\omega\epsilon_{eff}) \nabla u_0) = 0$$

$$\boldsymbol{\sigma_{eff} + i\omega\epsilon_{eff} = (\sigma_0 + i\omega\epsilon_0)\left(I + \upsilon M (I - \tfrac{\upsilon}{2} M)^{-1}\right) + o(\upsilon^2)}$$ and

$$\boldsymbol{M = \left(-\frac{d(\sigma_0 + i\omega\epsilon_0)}{(\sigma_m + i\omega\epsilon_m)} \int_{\Gamma/\upsilon} n_j \left(I + \frac{d(\sigma_0 + i\omega\epsilon_0)}{(\sigma_m + i\omega\epsilon_m)} \mathcal{L}_{\Gamma/\upsilon} \right)^{-1} [n_i] \right)}$$

Frequency-dependent behavior of $\sigma_{eff} + i\omega\epsilon_{eff}$

$\sigma_{eff} + i\omega\epsilon_{eff} = (\sigma_0 + i\omega\epsilon_0)\left(I + \upsilon M(I - \frac{\upsilon}{2}M)^{-1}\right) + o(\upsilon^2)$ and

$$M = \left(-\frac{d(\sigma_0 + i\omega\epsilon_0)}{(\sigma_m + i\omega\epsilon_m)} \int_{\Gamma/\upsilon} n_j \left(I + \frac{d(\sigma_0 + i\omega\epsilon_0)}{(\sigma_m + i\omega\epsilon_m)} \mathcal{L}_{\Gamma/\upsilon} \right)^{-1} [n_i] \right)$$

- Studies on determination of the effective property of a suspension: Maxwell, Poisson, Faraday, Rayleigh, Fricke, Lorentz, Debye, and Einstein.
- **Maxwell-Wagner-Fricke formula in the case of disk.**

$$M = \frac{2\pi r^3 d\omega(\epsilon_m\sigma_0 - \epsilon_0\sigma_m)}{(2r\sigma_m + \sigma_0 d)^2 + \omega^2(2r\epsilon_m + \epsilon_0 d)^2} I \qquad (r = \text{radius of disk})$$

$\rightsquigarrow$ **Debye relaxation time** $\tau = (2r\sigma_m + \sigma_0 d)/(2r\epsilon_m + \epsilon_0 d)$

- **Frequency-dependent anisotropy**:

$$\frac{\lambda_1(\omega)}{\lambda_2(\omega)} \approx 1 + (l_1 - l_2)\frac{2d\sigma_m\upsilon}{(\sigma_m^2 + \omega^2\epsilon_m^2)|\Gamma|} + O(d^2),$$

$\lambda_1 \leq \lambda_2$: eigenvalues of $\Im\{M(\omega)\}$ & $l_1 \leq l_2$: eigenvalues of $\int_{\Gamma/\upsilon} n\mathcal{L}_{\Gamma/\upsilon}[n]ds$.

Experiment: Apparent conductivity

In this experiment, the pointwise conductivity is $\sigma_{pt} = (1 + (10^{-8} - 1)\chi_C)$. The corresponding potential u_{pt} satisfies

$$\nabla \cdot ((1 + (10^{-8} - 1)\chi_C)\nabla u_{pt}) = 0 \quad \text{in } \Omega$$

where $C :=$ **thin film with holes**.

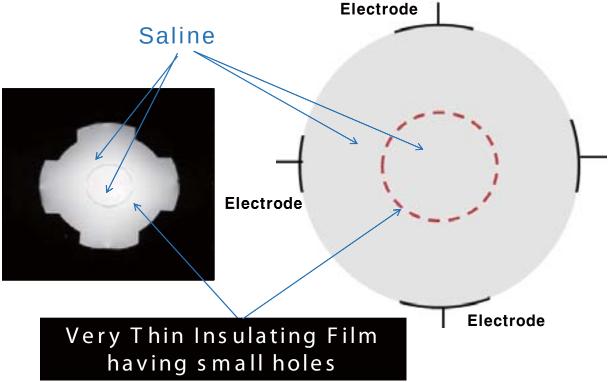

Apparent conductivity

The film is too thin to capture by any impedance imaging system. According to MREIT experiment, the reconstructed conductivity image is of the form:

$$\sigma_{apprent} = \begin{cases} \sigma_1 & \text{inside the film} \\ \sigma_2 & \text{outside the film} \end{cases}$$

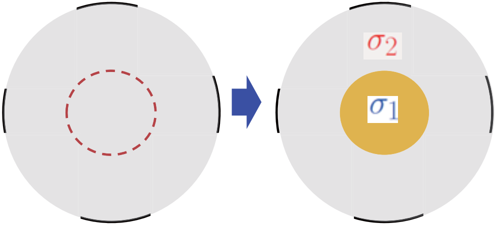

(Left) Pointwise conductivity (Right) Apparent conductivity

Apparent conductivity [Oh *et al* , PMB 2008]

The apparent conductivity by MREIT changes with the size of hole:

$$\nabla \cdot (\sigma \nabla u) = 0 \quad \text{in } \Omega \quad \sigma = \begin{cases} \sigma_1 & \text{inside the film} \\ \sigma_2 & \text{outside the film} \end{cases}$$

Bz data & Reconstructed Conudctivity distribution using MREIT

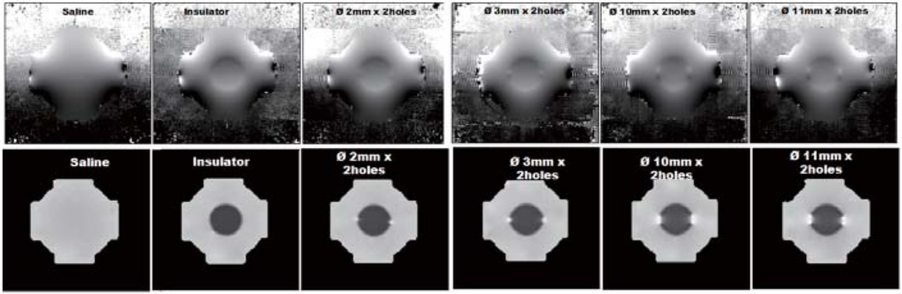

Ø of hole	Without hole	Ø 1mm	Ø 2mm	Ø 3mm	Ø 4mm	Ø 5mm	Ø 6mm	Ø 10mm
Conductivity change(%)	0	0.94	1.39	1.86	2.36	2.92	3.14	4.35

Conductivity changes with frequency. [IEEE TMI2012]

- **(Top)** Conductivity images at frequency **500 Hz** using MREIT.
- **(Bottom)** Conductivity images at frequency **126 MHz** using EPT.
- (Left) With insulating thin film & (Right) Without the film.
  - (Top-Left) **J** cannot pass through the thin insulating film.
  - (Bottom-Left) **J** can pass through the film.

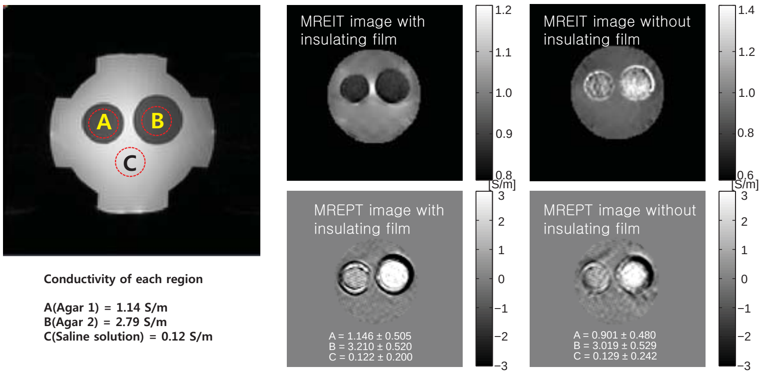

Issues in EIT.

✓ Bioimpedance spectroscopy can be used for clinical assessment of tissues since it reflects tissue composition variations, membrane characteristics, intra- and extracellular fluids and other factors.

✓ Can impedance imaging technique distinguish between carrot and cucumber? HOW?

- **Measuring frequency dependent behavior of effective conductivity increases distinguishability.**

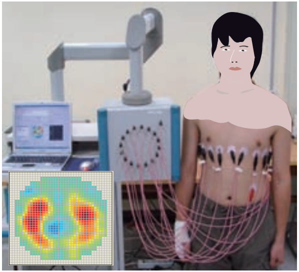

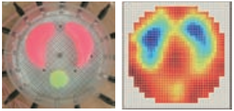

Time-difference EIT

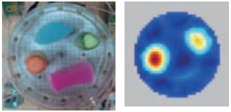

Frequency difference EIT

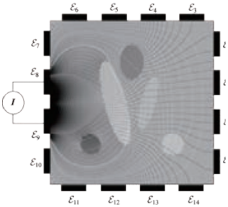

16 channel EIT

Electrical Impedance Tomography (EIT)

Aim: image internal admittivity distribution ($\gamma = \sigma + i\omega\epsilon$) from Nuemann-to-Dirichlet data measured by electrical electrodes on the boundary.

Zhang Tingting (张婷婷)

EIT Application: Lung Ventilation

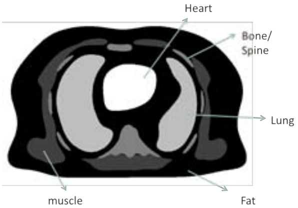

Load movie...

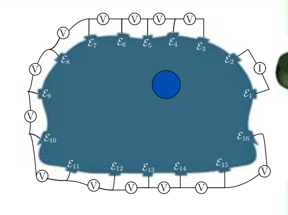

Adjacent pattern

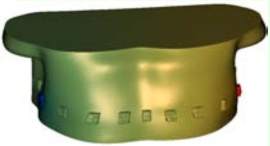

Forward solution u

Fat

Muscle

Rib/Bone

Heart&lung

Lung EIT in ICU and OR

- Life-saving of 1.1 million patients per year
- Cost-saving of US$ 3000 – 10,000 per patient

- Amato *et al.*, *New England Journal of Medicine*, 1998:338:347-54
- ARDS Network, *New England Journal of Medicine*, 2000:342:1301-8
- Rubenfeld *et al.*, *New England Journal of Medicine*, 2005:353:1685-93
- Wunsch *et al.*, *Critical Care Medicine*, 2010:38:1947-53

http://www.swisstom.com

Application of EIT: Obstructive Sleep Apnea

Experiment

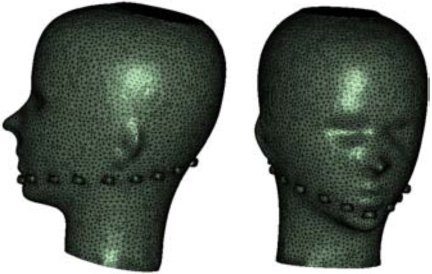

Electrodes configuration

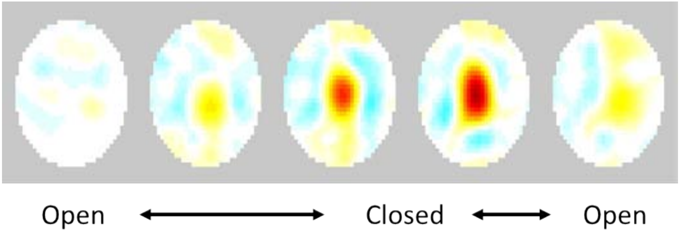

EIT Application: Spectroscopic Admittivity Imaging

Aim: determination of concrete cracks and reinforcing bars.

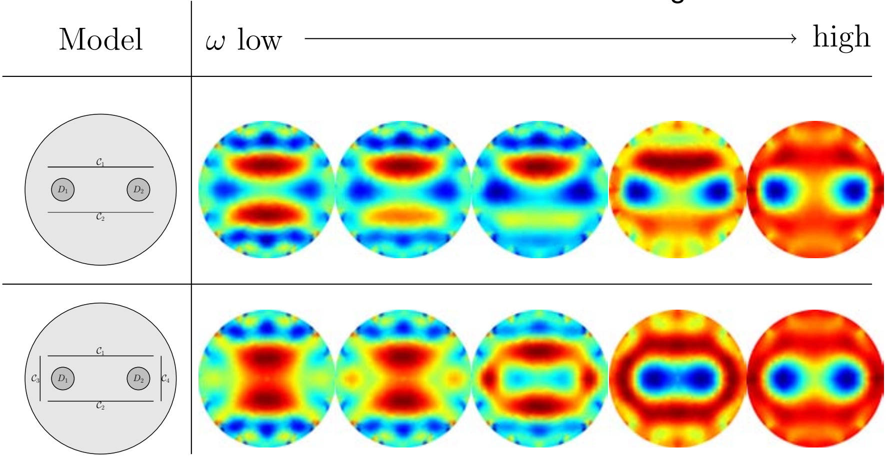

Two-dimensional Sensor using EIT

Chameleon TVR 2012 (PPS)

- 35,000,000 Won (40×40 cm2)
- Piezo-capacitive

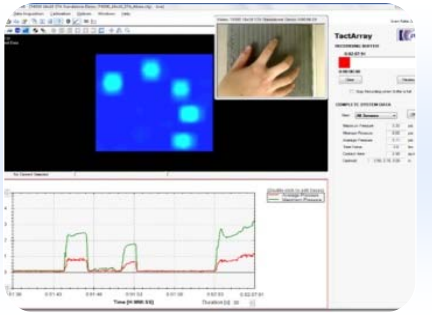

Emed (Novel)

- 150,000,000 Won (100×200 cm2)
- Piezo-capacitive

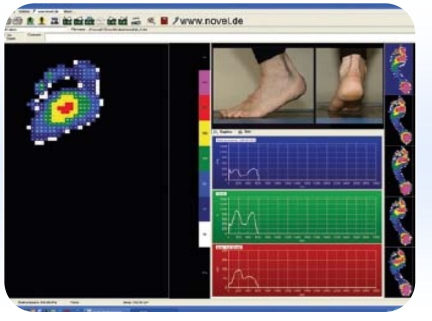

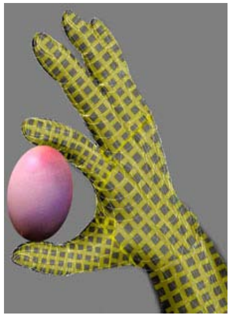

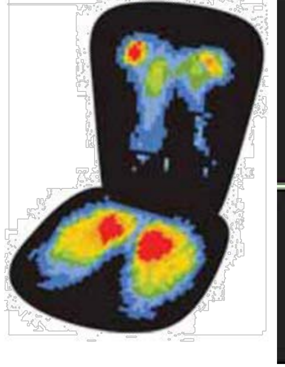

Two-dimensional Sensor using EIT

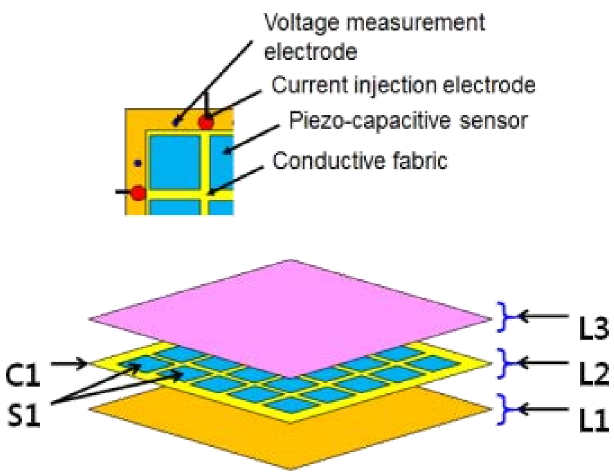

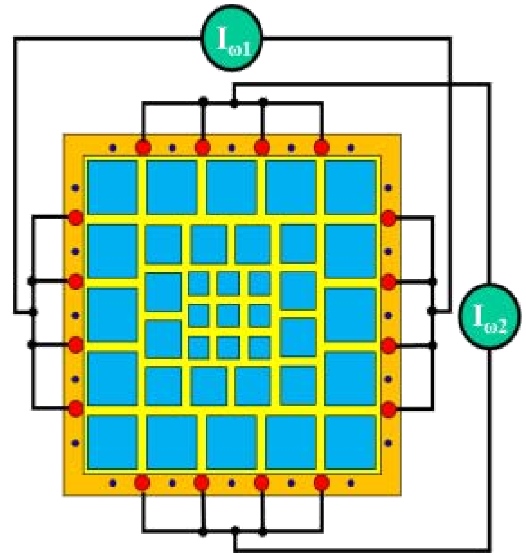

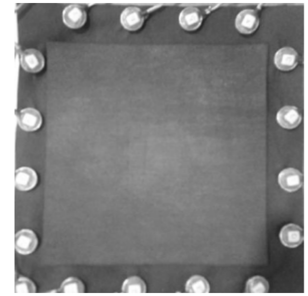

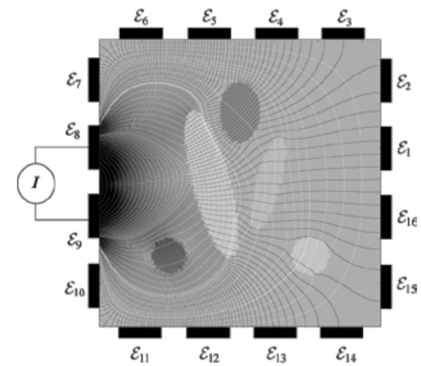

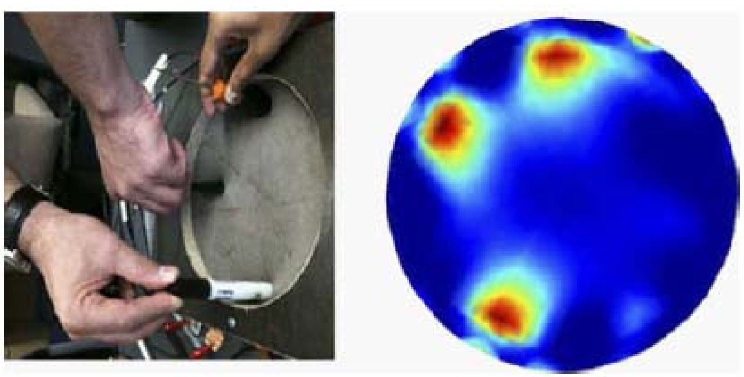

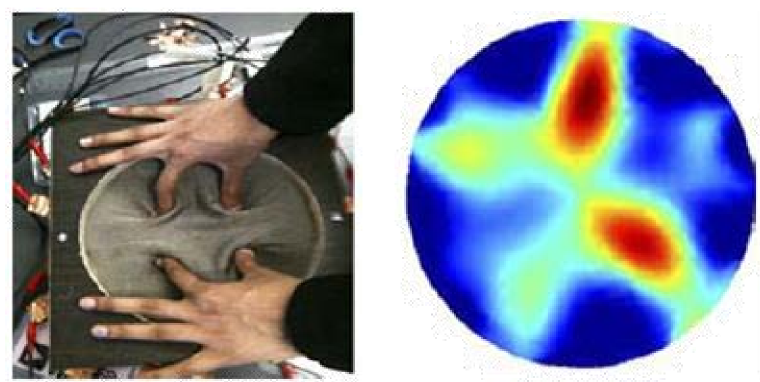

Electro-magnetic Tissue Property Imaging using MRI

✓ Experimental validation is needed to correct any mismatch between mathematical theory and experiment.

Electrodes

(recessed/hyrdogel)

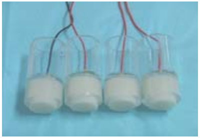

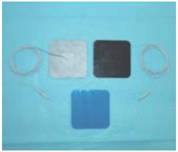

Imaging object

(Phantom/Animal)

Imgaing object

inside RF coil

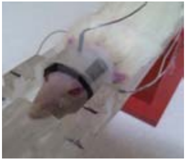

Electro-Magnetic Tissue Property Imaging

- Electromagnetic tissue properties include electrical conductivity σ, permittivity ϵ and magnetic susceptibility χ.
- Three methods were successful in experiments. Distributions of $\kappa = \sigma + i\omega\epsilon$ and χ in a subject are sources of magnetic field perturbations.

MREIT

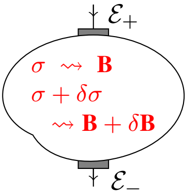

$$-\sigma\mathbf{E} = \nabla \times \mathbf{H}$$
$$\nabla \times \mathbf{E} = 0$$

MREPT

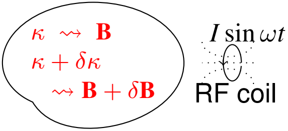

$$-\kappa\mathbf{E} = \nabla \times \mathbf{H}$$
$$\nabla \times \mathbf{E} = -i\omega\mathbf{B}$$

QSM

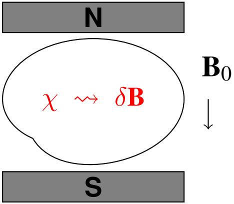

$$\mathbf{M} = \chi\mathbf{H}_0$$
$$\mathbf{M} \rightsquigarrow \delta\mathbf{B}$$

MREIT Math. Model

When modeling, we must take account of **well-posedness (Uniqueness, Existence, Stability)**.

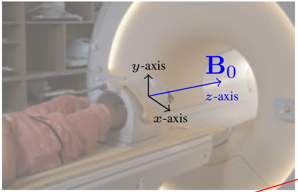

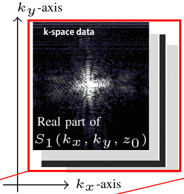

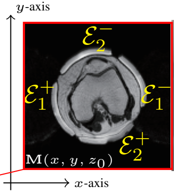

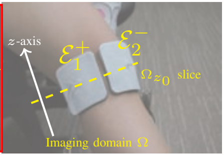

$$S_j(k_x, k_y, z_0) = \int_{\Omega_{z_0}} M(x, y, z_0) e^{i\delta(x,y,z_0)} e^{i\gamma T_c B_{z,j}(x,y,z_0)} e^{i(xk_x + yk_y)} dS_{xy}$$

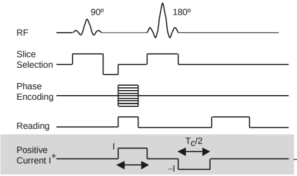

$$\frac{1}{\mu_0} \nabla \times \mathbf{B}_j = -\sigma \nabla u_j$$

$$I = \pm \int_{\mathcal{E}_j^{\pm}} \sigma \nabla u_j \cdot \mathbf{n} \, ds$$

$$(j = 1, 2)$$

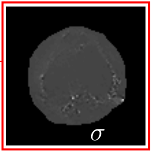

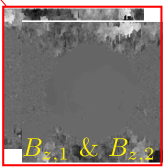

MREIT using full components of $\mathbf{H}$:

Major drawback: It requires subject rotation inside MRI scanner.

- Least square method
  [Zhang 1992]

$$\min_{\sigma} \frac{1}{2} \| \nabla \times \mathbf{H} + \sigma \nabla u \|^2$$

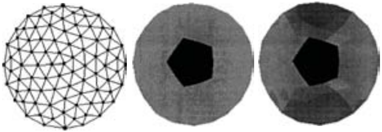

Finite element model   True $1/\sigma$ Reconstructed $1/\sigma$

Low spatial resolution

[Woo, Lee, Moon 1994], [Idel and Birgul 1995]

- $J-$substitution method
  [Kwon, Seo, Yoon, Woo 2001]

$$\nabla \cdot \left(\frac{|\mathbf{J}|}{|\nabla u|} \nabla u \right) = 0$$

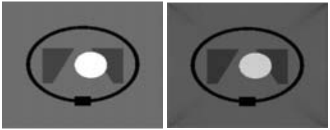

True $1/\sigma$ Reconstructed $1/\sigma$

High spatial resolution

In 2005-present, CDII by Nachman, Tamasan, Timonov, Joy

Drawback of MRCDII: Need to measure three components $\mathbf{B} = (B_x, B_y, B_z)$ to recover σ via $\nabla \cdot \left(\frac{|\nabla\times\mathbf{B}|}{|\nabla u|}\nabla u\right) = 0$. **However, MR scanner can measure only B_z.**

- **Measuring $\mathbf{B} = (B_x, B_y, B_z)$ requires impractical subject rotations.**
- **Serious practical difficulties arise from this requirement because of the limited space within the bore. Despite numerous attempts to overcome these difficulties, drawbacks remain, which seriously limit the clinical applicability of the method.**

According to Maxwell's eqn, $\mathbf{J}$ is directly related to $\mathbf{B} = (B_x, B_y, B_z)$, and σ must be computed from the relationship between $\mathbf{J}$ and $\mathbf{E}$. Therefore, B_z data alone were considered insufficient for conductivity image reconstructions, and conductivity imaging using B_z data alone appeared impossible until 2000.

Harmonic B_z-algorithm [2002; Seo, Kwon, Yoon, Woo]

The conductivity distribution σ can be reconstructed by only $\boldsymbol{B_z}$:

$$\nabla^2_{\mathrm{xy}} \ln \sigma(\mathbf{r}) = \nabla_{\mathrm{xy}} \cdot \left(\mathbf{A}^{\dagger}(\mathbf{r}) \begin{bmatrix} \nabla^2 B_{z,1}(\mathbf{r}) \\ \nabla^2 B_{z,2}(\mathbf{r}) \end{bmatrix} \right)$$

$$\text{where} \quad \mathbf{A}^{\dagger}(\mathbf{r}) := \frac{1}{\mu_0} \begin{bmatrix} \sigma \frac{\partial u_1[\sigma]}{\partial y}(\mathbf{r}) & -\sigma \frac{\partial u_1[\sigma]}{\partial x}(\mathbf{r}) \\ \sigma \frac{\partial u_2[\sigma]}{\partial y}(\mathbf{r}) & -\sigma \frac{\partial u_2[\sigma]}{\partial x}(\mathbf{r}) \end{bmatrix}^{-1}$$

This formula exists in an implicit form owing to the nonlinear relationship between σ and B_z, but it was designed to use a fixed-point theory. The major drawback of EIT, ill-posedness is mainly due to the fact that the overall flow of J is insensitive to local perturbations in σ. However, the harmonic Bz method takes advantage of this fact to make the algorithm work.

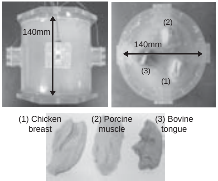

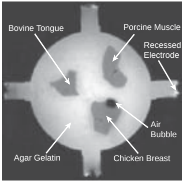

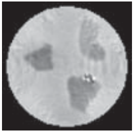

MREIT Images

MREIT is the most advanced conductivity imaging technique and now can offer state-of-the-art conductivity imaging for animal and human experiments. Until now, static EIT has not been successful in animal experiments.

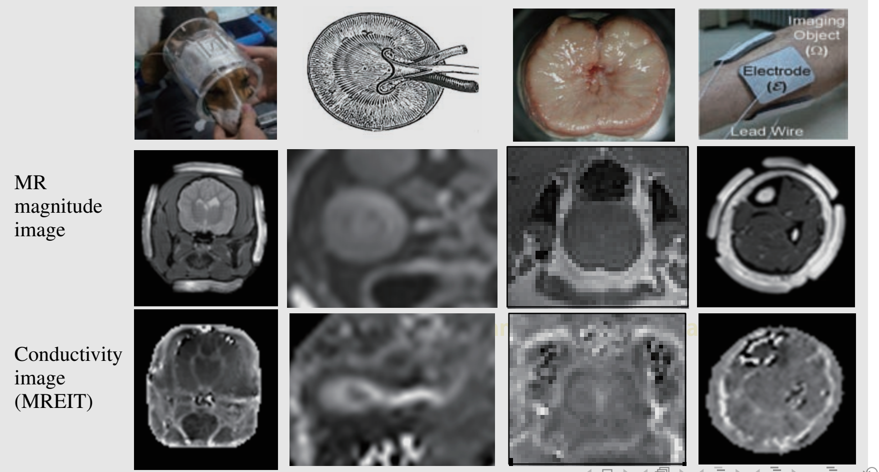

Magnetic Resonance Electrical Property Imaging

MREPT is a relatively new MR-based imaging modality to provide both conductivity (σ) and permittivity (ϵ) images at MR Larmor frequency (about 128 MHz at 3 Tesla MRI).

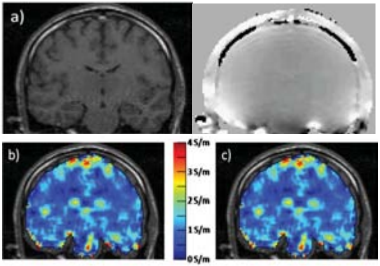

Conductivity

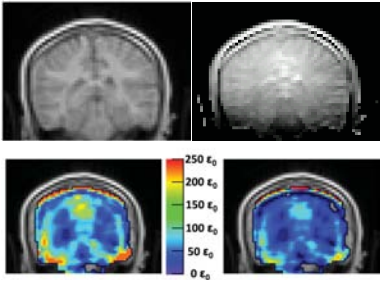

Permittivity

[Katscher *et al* IEEE TMI (2009)], $\frac{\omega}{2\pi}$ =128MHz

Refer the book "Electro-Magnetic Tissue Properties MRI" by [Seo, Woo, Katscher, Wang (2013)].

Measurable quantities in EPT [1]

- Using $B1$ mapping technique, we can measure the positive rotating magnetic field $H^{+} = \frac{1}{2}(H_x + iH_y)$ which is governed by

$$-\nabla^2 \mathbf{H} = \frac{\nabla\kappa}{\kappa} \times (\nabla \times \mathbf{H}) - i\omega\mu_0\kappa\mathbf{H}$$

- Unfortunately, we cannot measure $H^{-} = \frac{1}{2}(H_x - iH_y)$. Hence, each components H_x, H_y, H_z are not available.

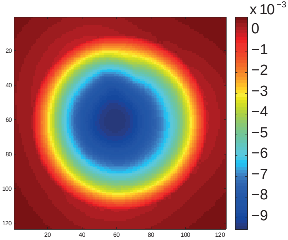

Real part of H^{+}

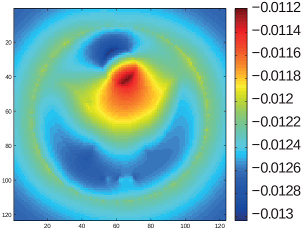

Imaginary part of H^{+}

[1] Stollberger and Wach 1996, Magn. Reson. Med.

Inverse problems of EPT

- Reconstruct the conductivity σ and permittivity ϵ (at frequency 126 MHz) from the given H^+ data and

$$-\nabla^2 \mathbf{H} = \underbrace{\frac{\nabla\kappa}{\kappa} \times (\nabla \times \mathbf{H})}_{\text{refraction term}} - i\omega\mu_0\kappa\mathbf{H}$$

※ Note that σ and ϵ (as effective properties) **change with** ω.

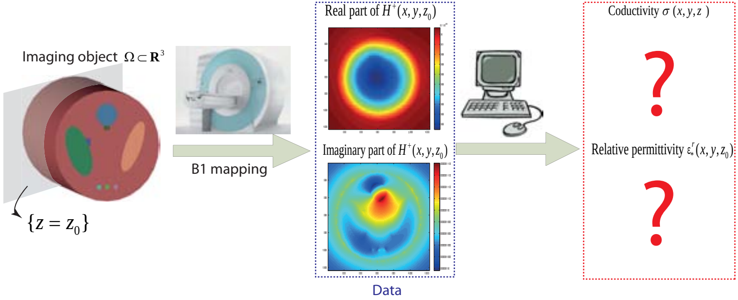

EPT-way of feeling admittivity

$H^+ = \frac{1}{2}(H_x + iH_y)$ probes $\kappa = \sigma + i\omega\epsilon$ through PDE

$$-\nabla^2 \underbrace{H^+(\mathbf{r})}_{Data} = \frac{1}{2}((\hat{\mathbf{x}} + i\hat{\mathbf{y}}) \times (\nabla \times \mathbf{H}(\mathbf{r}))) \cdot \nabla \underbrace{\ln \kappa}_{target} - i\omega\mu_0 \underbrace{\kappa}_{target} H^+(\mathbf{r}).$$

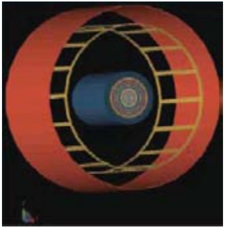

Experiment Setting

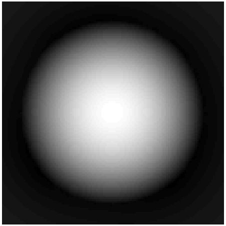

$\Re(H^+)$

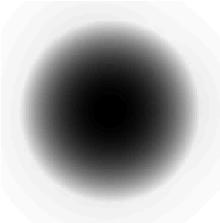

$\Im(H^+)$

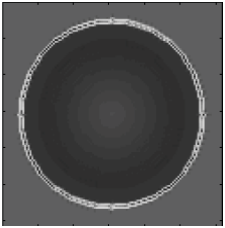

Target σ

[Haacke1991]

Why only $H^+ = H_x + iH_y$ is measurable quantity?

According to Faraday's law and reciprocity principle [Hoult2000], the induced RF-signal at the coil $\mathcal{C}$ is

$$\underbrace{\xi}_{RFsignal} := \oint_{\mathcal{C}} \mathbf{E^M} \cdot d\ell = -i\frac{\omega\mu_0}{I}\int_{\Omega} \mathbf{H}(\mathbf{r}) \cdot \mathbf{M}(\mathbf{r})\, d\mathbf{r}$$

- RF excitation with the main field $\mathbf{B}_0 = -B_0\hat{\mathbf{z}}$ generates magnetic field $\Re\{e^{i\omega_0 t}\mathbf{H}(\mathbf{r})\}$ (called $\mathbf{B}_1$-field) that is influenced by $\kappa = \sigma + i\omega\epsilon$. Here, $\omega_0 = \gamma B_0$ where γ is the gyromagnetic ratio.
- During RF excitation, $\Re\{e^{i\omega_0 t}\mathbf{M}(\mathbf{r}, t)\}$ precess according to Bloch equation $\frac{\partial}{\partial t}\Re\{e^{i\omega_0 t}\mathbf{M}(\mathbf{r}, t)\} = \Re\{e^{i\omega_0 t}\mathbf{M}(\mathbf{r}, t)\} \times \gamma(\mathbf{B}_0 + \Re\{e^{i\omega_0 t}\mathbf{H}(\mathbf{r})\})$.
- If we turn off RF field $\mathbf{H}$, $\mathbf{M}$ creates time-harmonic fields $\mathbf{H^M}$ and $\mathbf{E^M}$ that are dictated by $\nabla \times \mathbf{E^M} = -i\omega_0\mu_0(\mathbf{H^M} + \mathbf{M}) \quad \& \quad \nabla \times \mathbf{H^M} = \kappa\mathbf{E^M}$

Why is only H^+ measurable from RF signal?

Recalling that $\xi := \oint_{\mathcal{C}} \mathbf{E}^{\mathbf{M}} \cdot d\ell = -i\frac{\omega\mu_0}{I} \int_\Omega \mathbf{H}(\mathbf{r}) \cdot \mathbf{M}(\mathbf{r})\, d\mathbf{r}$, the following NMR RF signal for each angle α is measurable:

$$\xi_\alpha(\mathbf{r}) := 2C_1 M_0(\mathbf{r}) H^-(\mathbf{r}) \left(\sin\left(C_2\alpha|H^+(\mathbf{r})|\right) \frac{H^+(\mathbf{r})}{|H^+(\mathbf{r})|} \right).$$

- The transverse field $\mathbf{H}_{xy} = H_x\hat{\mathbf{x}} + H_y\hat{\mathbf{y}}$ can be decomposed into $\mathbf{H}_{xy} = \frac{H_x - iH_y}{2}\mathbf{a}_+ + \frac{H_x - iH_y}{2}\mathbf{a}_- = H^+\mathbf{a}_+ + H^-\mathbf{a}_-$ where $\mathbf{a}_\pm = \hat{\mathbf{x}} \mp i\hat{\mathbf{y}}$.
- The transversal component $\mathbf{M}_{xy} = M_x\hat{\mathbf{x}} + M_y\hat{\mathbf{y}}$ interact with H^+ components and it can be approximated by $\mathbf{M}_{xy}(\mathbf{r}) \approx \; C_1 M_0(\mathbf{r}) \left(\sin\left(C_2\alpha|H^+(\mathbf{r})|\right) \frac{H^+(\mathbf{r})}{|H^+(\mathbf{r})|} \right) \mathbf{a}_+$.
- The identity follows from $\mathbf{a}_- \cdot \mathbf{a}_- = 0 \;\&\; \mathbf{a}_- \cdot \mathbf{a}_+ = 2$.

⁂ In MRI community, H^+ with $\mathbf{B}_0$ being positive z-direction is known as measurable quantity. But that is NOT true. The truth is that H^- is measurable quantity.

Conventional method : Ignore the refraction term

$$-\nabla^2\mathbf{H} = \underbrace{\frac{\nabla\kappa}{\kappa} \times (\nabla \times \mathbf{H})}_{\text{refraction term}} - i\omega\mu_0\kappa\mathbf{H}$$

- Wen (2003) uses the assumption of **local homogeneity** of κ to get

$$\kappa(\mathbf{r}) = \frac{i}{\omega\mu_0}\frac{\nabla^2 H^+(\mathbf{r})}{H^+(\mathbf{r})}$$

- Katscher *et al* (2009) performed initial experiments on a standard clinical MRI system: For any disk $D_\delta(\mathbf{r}_0) \subset \Omega$ where $\nabla\kappa \approx 0$,

$$\kappa = \frac{\oint_{\partial D_{\mathbf{r}}} \nabla \times \mathbf{H} \cdot d\ell}{i\mu_0\omega \int_{D_{\mathbf{r}}} \mathbf{H} \cdot dS}.$$

In the locally homogeneous region $(\nabla\kappa \approx 0)$,

$$-\nabla^2\mathbf{H} = \underbrace{\nabla \ln\kappa \times \nabla \times \mathbf{H}}_{=0} - i\mu_0\omega\kappa\mathbf{H} \quad \Rightarrow \quad \kappa = \frac{1}{i\omega\mu_0}\frac{\nabla^2 H^+}{H^+}$$

This formula does not work when evaluating small conductivity anomalies.

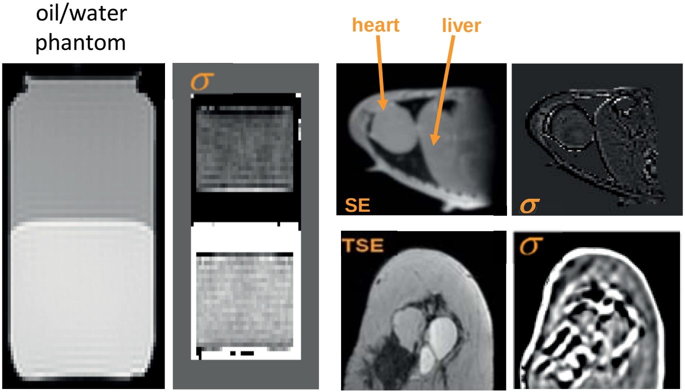

Direct reconstruction formula $\kappa = \frac{1}{i\omega\mu_0}\frac{\nabla^2 H^+}{H^+}$

- Neglecting $\nabla \ln \kappa(\mathbf{r}) \times [\nabla \times \mathbf{H}(\mathbf{r})]$ causes serious artifacts.

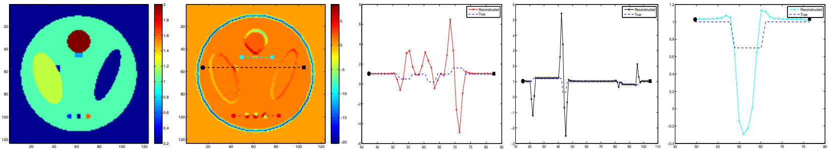

True conductivity $\sigma_*(x,y,z_0)$ | Reconstructed conductivity $\sigma(x,y,z\ )$ | Profile along the red line in $\sigma(x,y,z_0)$ | Profile along the black line in $\sigma(x,y,z_0)$ | Profile along the cyan line in $\sigma(x,y,z_0)$

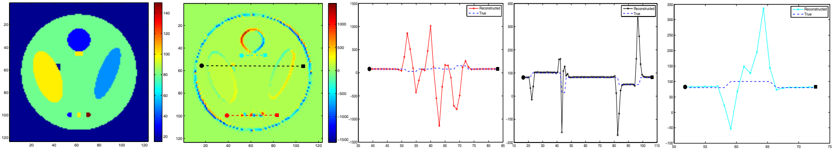

True relative permittivity $\varepsilon_*^r(x,y,z_0)$ | Reconstructed relative permittivity $\varepsilon^r(x,y,z_0)$ | Profile along the red line in $\varepsilon^r(x,y,z_0)$ | Profile along the black line in $\varepsilon^r(x,y,z_0)$ | Profile along the cyan line in $\varepsilon^r(x,y,z_0)$

Figure shows that the direct method produces serious errors near small anomalies.

Error analysis: Direct formula $\kappa^* = \frac{1}{i\omega\mu_0}\frac{\nabla^2 H^+}{H^+}$

$$\text{Error} = \kappa - \kappa^* = \left(\frac{1}{i\omega\mu_0}\frac{\nabla^2 H^+}{H^+} - \frac{\nabla^2 H^-}{i\omega\mu_0 H^-}\right)\left[1 - \frac{H^+\frac{\partial}{\partial z}H^-}{H^-\frac{\partial}{\partial z}H^+}\right]^{-1}$$

where $\mathbf{H} = (H^+ + H^-, -iH^+ + iH^-, H_z)$.

MREPT

MREIT

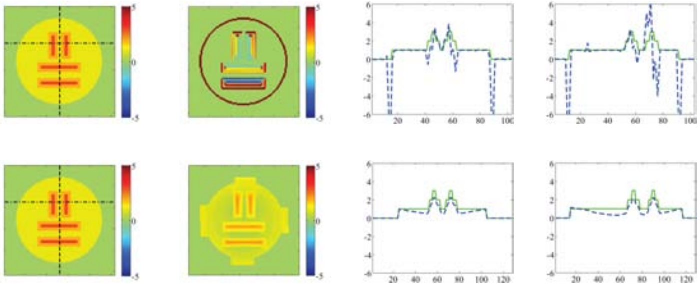

Phantom Model | Reconstruction | Horizontal axis | Vertical axis

[Seo *et al* IEEE TMI 2012]

We should include the refraction term $\nabla \ln \kappa(\mathbf{r}) \times [\nabla \times \mathbf{H}(\mathbf{r})]$ in the reconstruction algorithm

Theorem (Govern equation: Y. Song & S, (SIAM AP2013))

Assume $H_z = 0$. The admittivity κ satisfies the equation

$$\mathbf{V}_{H^+}(\mathbf{r}) \cdot \nabla \ln \kappa(\mathbf{r}) - i\omega\mu_0 H^+(\mathbf{r})\kappa(\mathbf{r}) = -\nabla^2 H^+(\mathbf{r}) \qquad \textit{for } \mathbf{r} \in \Omega \qquad (\clubsuit)$$

where $\mathbf{V}_{H^+} := -\left(2\partial H^+, 2i\partial H^+, \frac{\partial H^+}{\partial z}\right)$ & $\partial = \frac{1}{2}(\frac{\partial}{\partial x} - i\frac{\partial}{\partial y})$.

- This first-order PDE may not be solvable for κ since the direction vector field $\mathbf{V}_{H^+}$ is not real-valued function. The method of characteristics can not be applied. Indeed, Hörmander and Lewy provided non-existence results for the first order PDE with complex-valued coefficients.

Degenerate Elliptic PDE[Kwon *et al* 2014]

Theorem

The distributions of σ *and* ϵ *satisfy the following equation:*

$$\nabla \cdot \left(A[H^+] \nabla \begin{pmatrix} \sigma \\ \omega\epsilon \end{pmatrix} \right) + F_0[H^+] \cdot \nabla \begin{pmatrix} \sigma \\ \omega\epsilon \end{pmatrix} = \begin{pmatrix} F_1[\sigma, \epsilon, H^+] \\ F_2[\sigma, \epsilon, H^+] \end{pmatrix} \quad \textit{in } \Omega,$$

where $A[H^+]$ *is a positive semi-definite matrix given by*

$$A[H^+] = \begin{bmatrix} P_x^2 + P_y^2 & 0 & P_xP_z + P_yQ_z \\ 0 & P_x^2 + P_y^2 & P_yP_z - P_xQ_z \\ P_xP_z + P_yQ_z & P_yP_z - P_xQ_z & P_z^2 + Q_z^2 \end{bmatrix} \quad \textit{in } \Omega.$$

$$P = (P_x, P_y, P_z) = \left(-\frac{\partial}{\partial x} H_r^+ - \frac{\partial}{\partial y} H_i^+,\ \frac{\partial}{\partial x} H_i^+ - \frac{\partial}{\partial y} H_r^+,\ -\frac{\partial}{\partial z} H_r^+ \right),$$

$$Q = (Q_x, Q_y, Q_z) = \left(\frac{\partial}{\partial x} H_i^+ - \frac{\partial}{\partial y} H_r^+,\ \frac{\partial}{\partial x} H_r^+ + \frac{\partial}{\partial y} H_i^+,\ \frac{\partial}{\partial z} H_i^+ \right),$$

$$E[\eta, H^+] = Q[H^+] \cdot \nabla(P[H^+] \cdot \nabla\eta) - P[H^+] \cdot \nabla(Q[H^+] \cdot \nabla\eta),$$

$$\phi = \omega\mu_0 H_i^+ \sigma^2 - \omega\mu_0 H_i^+ \epsilon^2 + 2\omega\mu_0 H_r^+ \sigma\epsilon + \Delta H_r^+ \sigma - \omega \Delta H_i^+ \epsilon,$$

$$\psi = -\omega\mu_0 H_r^+ \sigma^2 + \omega\mu_0 H_r^+ \epsilon^2 + 2\omega\mu_0 H_i^+ \sigma\epsilon + \Delta H_i^+ \sigma + \omega \Delta H_r^+ \epsilon.$$

Results: Solving degenerate elliptic PDE

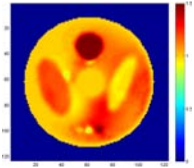

it5: Conductivity

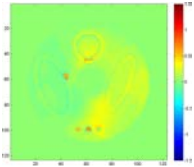

Error

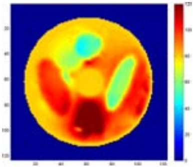

Permittivity

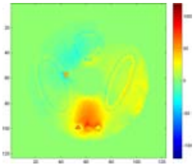

Error

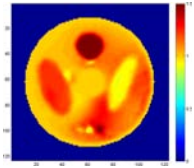

it10: Conductivity

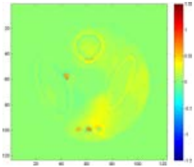

Error

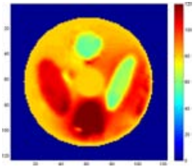

Permittivity

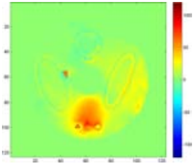

Error

Quantitative Susceptibility Mapping (QSM)

QSM: aims to visualize **magnetic susceptibility** χ from MR data.

- **Magnetic susceptibility** χ: an intrinsic property of the material relating the magnetization $\mathbf{M}$ and the magnetic field $\mathbf{H}$ via $\mathbf{M} = \chi\mathbf{H}$.

Applications of QSM: Disease diagnosis (Parkinson's, Alzheimer, stroke, blood calcification, etc.)

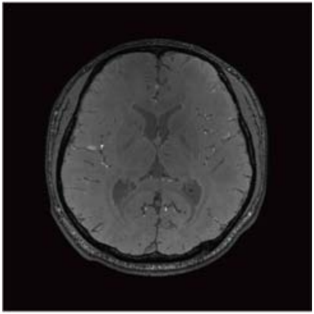

MR Magnitude Image

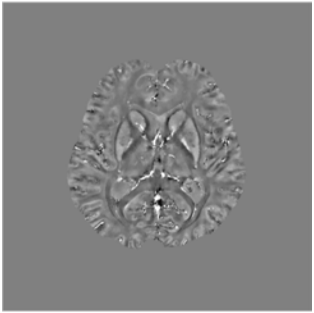

Susceptibility Image

Inverse Problem of QSM

- Solve the deconvolution problem for χ:

$$\psi(\mathbf{x}) = \mathrm{pv}\int_{\mathbb{R}^3} d(\mathbf{x}-\mathbf{y})\chi(\mathbf{y})d\mathbf{y} \qquad d(\mathbf{x}) = \frac{2x_3^2 - x_1^2 - x_2^2}{4\pi|\mathbf{x}|^5}$$

$$\underbrace{\Psi(\boldsymbol{\xi})}_{\mathcal{F}(\psi)(\boldsymbol{\xi})} = \left(\frac{1}{3} - \frac{\xi_3^2}{|\boldsymbol{\xi}|^2}\right) \underbrace{\mathcal{X}(\boldsymbol{\xi})}_{\mathcal{F}(\chi)(\boldsymbol{\xi})} = \mathcal{D}(\boldsymbol{\xi})\mathcal{X}(\boldsymbol{\xi}).$$

(pv: the principal value of the integral, $\mathcal{F}$: Fourier transform)

- Data: relative difference field (RDF) ψ (noisy)
- Integral kernel d: singular $(d(r\mathbf{x}) = r^{-3}d(\mathbf{x})$ for $r > 0)$.

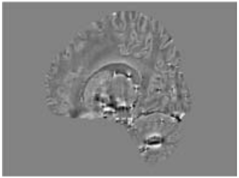

Data ψ (Noisy)

$=$

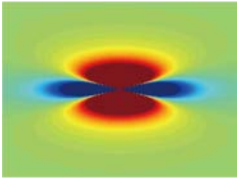

Unit dipole field d

$*$

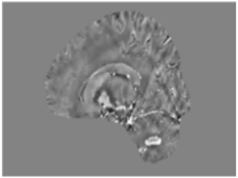

Susceptibility χ

Challenging Issue

$$\psi(\mathbf{x}) = \mathrm{pv}\int_{\mathbb{R}^3} d(\mathbf{x}-\mathbf{y})\chi(\mathbf{y})d\mathbf{y} \qquad \text{(IP-I)}$$

$$\underbrace{\Psi(\boldsymbol{\xi})}_{\mathcal{F}(\psi)(\boldsymbol{\xi})} = \underbrace{\left(\frac{1}{3} - \frac{\xi_3^2}{|\boldsymbol{\xi}|^2}\right)}_{\mathcal{D}(\boldsymbol{\xi})} \underbrace{\mathcal{X}(\boldsymbol{\xi})}_{\mathcal{F}(\chi)(\boldsymbol{\xi})} \qquad \text{(IP-F)}$$

ill-posed since

$$\mathcal{D}(\boldsymbol{\xi}) = 0 \ \text{ in } \ \Gamma_0 = \{\boldsymbol{\xi} \in \mathbb{R}^3 : \xi_1^2 + \xi_2^2 - 2\xi_3^2 = 0\},$$

and this leads to the **streaking artifacts.**

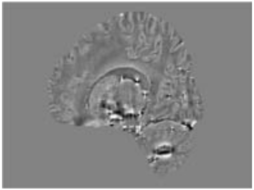

Data ψ

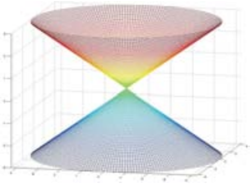

Γ_0 in Fourier domain

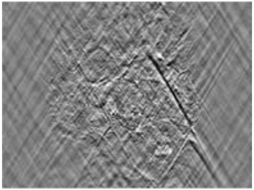

Reconstructed χ using (IP-F)

Source of Error Propagation

- For a given measurement $\psi \in \mathcal{E}'$, we aim to obtain $\chi \in \mathcal{E}'$ using (IP-I) or (IP-F):

$$\psi(\mathbf{x}) = \lim_{\varepsilon \searrow 0} \int_{|\mathbf{x}-\mathbf{y}|>\varepsilon} d(\mathbf{x}-\mathbf{y})\chi(\mathbf{y})d\mathbf{y} \qquad \text{(IP-I)}$$

$$\Psi(\boldsymbol{\xi}) = \mathcal{D}(\boldsymbol{\xi})\mathcal{X}(\boldsymbol{\xi}) = \left(\frac{1}{3} - \frac{\xi_3^2}{|\boldsymbol{\xi}|^2}\right)\mathcal{X}(\boldsymbol{\xi}) \qquad \text{(IP-F).}$$

($\mathcal{D}'$: space of distributions, $\mathcal{E}'$: space of compactly supported distributions, $\mathcal{S}'$: space of tempered distributions)

- If $\psi \in \mathcal{E}'$ satisfies (IP-F) for some $\chi \in \mathcal{E}'$, then ψ must lie in

$$\mathcal{E}'_\diamondsuit := \left\{u \in \mathcal{E}' : \widehat{u}(\boldsymbol{\xi})/P(\boldsymbol{\xi}) \text{ is bounded near } \Gamma_0\right\}.$$

Here, $P(\boldsymbol{\xi})$ is the polynomial defined as

$$P(\boldsymbol{\xi}) = \frac{4\pi^2}{3}(\xi_1^2 + \xi_2^2 - 2\xi_3^2).$$

Theorem (Existence and Uniqueness [J.K.Choi *et al* . 2014.])

If $\psi \in \mathcal{E}'_{\diamondsuit}$, *we have the* ***unique*** $\chi \in \mathcal{E}'$ *satisfying (IP-F), and* $\mathcal{X} = \mathfrak{F}(\chi)$ *can be represented as*

$$\mathcal{X}(\boldsymbol{\xi}) = \begin{cases} \dfrac{4\pi^2|\boldsymbol{\xi}|^2\Psi(\boldsymbol{\xi})}{P(\boldsymbol{\xi})} & \textit{if } \boldsymbol{\xi} \notin \Gamma_0 \\[2ex] -\dfrac{9\xi_3}{4}\dfrac{\partial\Psi}{\partial\xi_3}(\boldsymbol{\xi}) & \textit{if } \boldsymbol{\xi} \in \Gamma_0 \setminus \{\mathbf{0}\}. \end{cases} \qquad (\clubsuit)$$

(Proof follows from Paley-Wiener-Schwartz theorem.)


Reference χ


$\psi \in \mathcal{E}'_{\diamondsuit}$

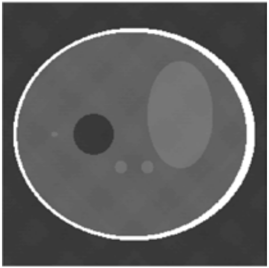
Reconstructed χ using ($\clubsuit$)

Cause of Streaking Artifacts

- **Streaking artifacts: closely related with the PDE**

$$P(D)\chi = \left(-\frac{1}{3}\Delta + \frac{\partial^2}{\partial x_3^2}\right)\chi = -\Delta\psi \qquad \text{(IP-PDE)}$$

- The solution $\chi^\sharp \in \mathcal{D}'$ to (IP-PDE) is expressed as

$$\chi^\sharp(\mathbf{x}) = E * (-\Delta\psi)(\mathbf{x}) = -\int_{\mathbb{R}^3} E(\mathbf{x}-\mathbf{y})\Delta_{\mathbf{y}}\psi(\mathbf{y})d\mathbf{y} \qquad \psi \in \mathcal{E}' \qquad \text{(S-PDI}$$

where $E(\mathbf{x})$ is the fundamental solution of $P(D)$:

$$E(\mathbf{x}) = \begin{cases} \dfrac{3}{4\pi\sqrt{x_3^2 - 2(x_1^2 + x_2^2)}} & \text{if } 2(x_1^2 + x_2^2) < x_3^2 \\ 0 & \text{otherwise.} \end{cases}$$

$E(\mathbf{x})$ has the singular support along $\{\mathbf{x} \in \mathbb{R}^3 : 2(x_1^2 + x_2^2) = x_3^2\}$.

Microlocal Analysis of Inverse Problem

Key Observation

To analyze the streaking artifacts in an image, **simultaneous concentration on both image and its Fourier transform** is crucial.

Definition

Wave front set of $u \in \mathcal{D}'$: a closed conic set in $\mathbb{R}^3 \times (\mathbb{R}^3 \setminus \{\mathbf{0}\})$

$$\mathrm{WF}(u) = \left\{(\mathbf{x}, \boldsymbol{\xi}) \in \mathbb{R}^3 \times (\mathbb{R}^3 \setminus \{\mathbf{0}\}) : \boldsymbol{\xi} \in \Sigma_{\mathbf{x}}(u)\right\}.$$

$\boldsymbol{\xi} \notin \Sigma_{\mathbf{x}}(u) \iff \exists \varphi \in C_c^\infty$ with $\varphi(\mathbf{x}) \neq 0$ and a conic nbd V of $\boldsymbol{\xi}$ s.t.

$$\sup_{\boldsymbol{\eta} \in V} (1 + |\boldsymbol{\eta}|)^N |\widehat{\varphi u}(\boldsymbol{\eta})| < \infty \qquad \forall N \in \mathbb{N}.$$

If $(\mathbf{x}, \boldsymbol{\xi}) \in \mathrm{WF}(u)$, then

- $\mathbf{x} \in \text{sing-supp}(u) \implies$ **location of singularity**
- $\boldsymbol{\xi} \in \Sigma_{\mathbf{x}}(u) \implies$ **cause of singularity**

Theorem (Characterization of Artifacts [J.K.Choi *et al* . 2014.])

For $\psi \in \mathcal{E}'$*, the wave front set of* $\chi = \chi^\sharp$ *satisfies*

$$\mathrm{WF}(\chi) \setminus \mathrm{WF}(\psi) \subseteq \big\{(t\nabla P(\boldsymbol{\xi}) + \mathbf{x}, \boldsymbol{\xi}) : \boldsymbol{\xi} \in \Gamma_0 \setminus \{\mathbf{0}\},\ t \neq 0,\ (\mathbf{x}, \boldsymbol{\xi}) \in \mathrm{WF}(\psi)\big\}$$

Moreover, if $(\mathbf{x}, \boldsymbol{\xi}) \in \mathrm{WF}(\chi) \setminus \mathrm{WF}(\psi)$*, then*

- $\boldsymbol{\xi} \in \Gamma_0$
- *for any open interval* (a, b) *containing* 0 *such that* $\big\{(\mathbf{x} + t\nabla P(\boldsymbol{\xi}), \boldsymbol{\xi}) : t \in (a, b)\big\} \cap \mathrm{WF}(\psi) = \emptyset$*, we have*

$$\big\{(\mathbf{x} + t\nabla P(\boldsymbol{\xi}), \boldsymbol{\xi}) : t \in (a, b)\big\} \subseteq \mathrm{WF}(\chi).$$

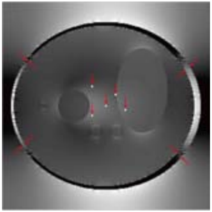

Simulated $\psi \in \mathcal{E}' \setminus \mathcal{E}'_\diamond$

Fundamental solution E

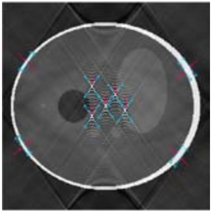

$\chi^\sharp = E * (-\Delta\psi)$

Regularization

- **Reduces streaking artifacts** using total variation and wavelet $\mathbf{\Phi}$:

$$\chi = \arg\min \ \alpha\|\chi\|_{\mathrm{TV}} + \beta\|\mathbf{\Phi}\chi\|_1 + \frac{1}{2}\|\mathcal{D}\mathcal{F}(\chi) - \Psi\|^2_{L^2} \qquad \textbf{[TVL1L2]}$$

[B.Wu *et al* . 2012]

- May **lack realistic variations** (in the case of real measured data)

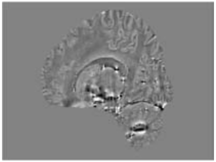

Measured $\psi \in \mathcal{E}'$

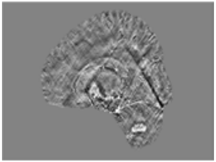

TKD $(\hbar = 0.08)$

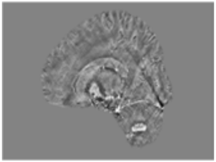

TKD $(\hbar = 0.16)$

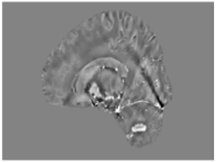

[TVL1L2] $(\alpha = \beta = 0.0005)$

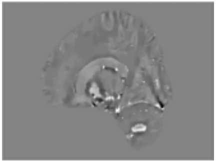

[TVL1L2] $(\alpha = \beta = 0.002)$

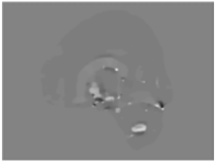

[TVL1L2] $(\alpha = \beta = 0.008)$

Morphology Enabled Bayesian Approach

- **Spatial priors** can be used to improve **[TVL1L2]**:

$$\chi = \arg\min \; \alpha\|\mathfrak{M}\nabla\chi\|_1 + \frac{1}{2}\|\mathfrak{W}(d * \chi - \psi)\|_{L^2}^2 \qquad \textbf{[MEDI]}$$

[T.Liu *et al* . 2009] $\mathfrak{M}$: structural weighting matrix, $\mathfrak{W}$: noise weighting matrix

- Improve **morphological information**
- Obtain weighting matrices **empirically**

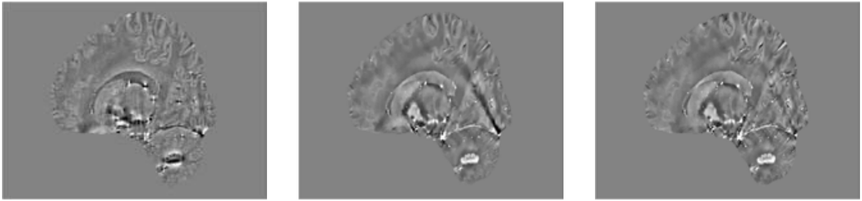

Measured $\psi \in \mathcal{E}'$ | **[TVL1L2]** $(\alpha = \beta = 0.0005)$ | **[MEDI]** $(\alpha = 0.0005)$

MR elastography (with Liangdong Zhou)

- Inaccurate, Qualitative VS. Accurate, Quantitative[2]

Palpation

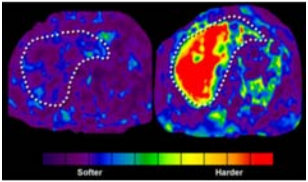

Elastography

- Elastography generation procedure[3]:

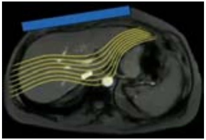

Vibration

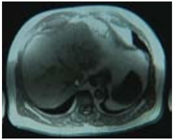

MRI

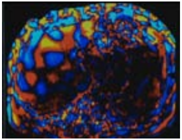

Displacement

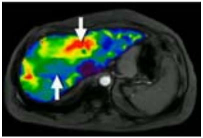

Elastography

2 http://www.drbambach.de and http://parade.condenast.com
3 http://www.mayoclinic.org/

Mathematical Model

For linearly incompressible, viscoelastic object $\Omega \in \mathbb{R}^2$, when we apply the time-harmonic vibrations through the boundary, the induced internal displacement field $\mathbf{u}$ satisfies

$$\nabla \cdot ((\mu + i\omega\eta_\mu)(\nabla \mathbf{u} + \nabla \mathbf{u}^t)) + \underbrace{\nabla((\lambda + i\omega\eta_\lambda)\nabla \cdot \mathbf{u})}_{Trouble!!!} + \rho\omega^2 \mathbf{u} = 0$$

- Note that the medium is incompressible ($\nabla \cdot \mathbf{u} \approx 0$) and $\lambda \approx \frac{3\mu\nu}{(1-2\nu)(1+\nu)} \approx \infty$ for Poisson ratio $\nu \approx 0.5$,
- Denote the internal pressure $p = \lambda \nabla \cdot \mathbf{u}$ in the limit sense $p = \lim_{\lambda \to \infty, \nabla \cdot \mathbf{u} \to 0} \lambda \nabla \cdot \mathbf{u}$ and strain tensor $\nabla^s \mathbf{u} = \frac{1}{2}(\nabla \mathbf{u} + \nabla \mathbf{u}^t)$.
- We have forward problem in the above sense

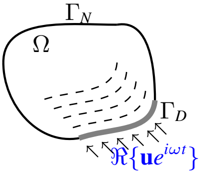

Figure 1: time harmonic vibration model

$$\begin{cases} 2\nabla \cdot (\mu + i\omega\eta_\mu)\nabla^s \mathbf{u} + \nabla p + \rho\omega^2 \mathbf{u} = 0 & \text{in } \Omega, \\ \nabla \cdot \mathbf{u} = 0 \quad \text{in } \Omega, \\ \mathbf{u} = \mathbf{g} \quad \text{on } \Gamma_D, \\ 2(\mu + i\omega\eta_\mu)\nabla^s \mathbf{u}\mathbf{n} + p\mathbf{n} = 0 & \text{on } \Gamma_N. \end{cases}$$

The inverse problem is to reconstruct μ and η_μ with measured data $\mathbf{u}_m$.

Adjoint-based Optimization Reconstruction

- Define the discrepancy functional and do minimization:

$$J[\mu, \eta_\mu] = \frac{1}{2} \int_\Omega |\mathbf{u}[\mu, \eta_\mu] - \mathbf{u}_m[\mu^*, \eta_\mu^*]|^2 dx.$$

- We introduce the following adjoint problem

$$\begin{cases} 2\nabla \cdot (\mu - i\omega\eta_\mu)\nabla^s \mathbf{v} + \nabla q + \rho\omega^2 \mathbf{v} = (\mathbf{u} - \mathbf{u}_m) & \text{in } \Omega, \\ \nabla \cdot \mathbf{v} = 0 \quad \text{in } \Omega, \\ \mathbf{v} = 0 \quad \text{on } \Gamma_D, \\ 2(\mu - i\omega\eta_\mu)\nabla^s \mathbf{v}\mathbf{n} + q\mathbf{n} = 0 \quad \text{on } \Gamma_N. \end{cases}$$

Theorem (Fréchet derivatives)

Fréchet derivatives of $J[\mu, \eta_\mu]$ in μ and η_μ:

$$\frac{\partial}{\partial \mu} J[\mu, \eta_\mu] = \Re\left[2\nabla^s \mathbf{u} : \nabla^s \bar{\mathbf{v}} dx\right],$$

$$\frac{\partial}{\partial \eta_\mu} J[\mu, \eta_\mu] = \Re\left[2(i\omega\nabla^s \mathbf{u}) : \nabla^s \bar{\mathbf{v}} dx\right].$$

Theorem (Iterative scheme)

With proper initial guess $\mu^0 + i\eta_\mu^0$, we have

$$\mu^{m+1} = \mu^m - \delta \frac{\partial J}{\partial \mu}(\mu^m, \eta_\mu^m),$$

$$\eta_\mu^{m+1} = \eta_\mu^m - \delta \frac{\partial J}{\partial \eta_\mu}(\mu^m, \eta_\mu^m).$$

Numerical Results: Reconstruction in whole domain

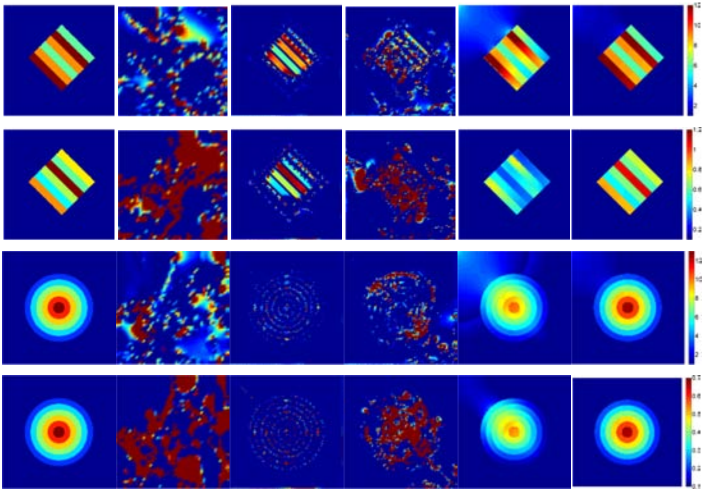

(a) (b) (c) (d) (e) (f)

(a) True images; (b) reconstruction with homogeneous initial guess; (c) direct inversion method; (d) reconstruction with initial guess (c); (e) hybrid one-step method; (f) reconstruction with initial guess (e).

Numerical Results: Reconstruction in local domain

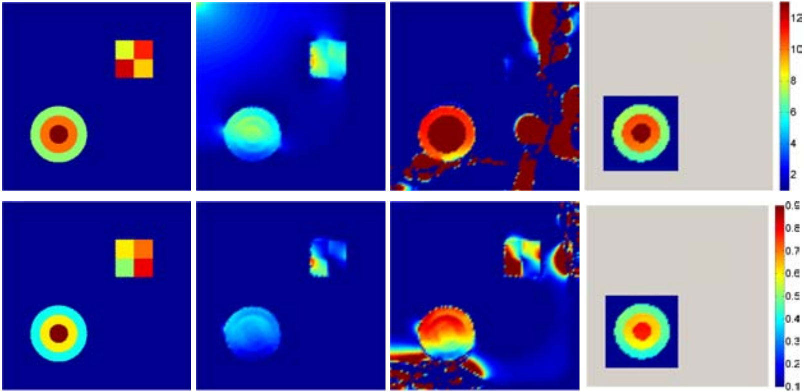

(a) (b) (c) (d)

(a) True images; (b) hybrid one-step method; (c) reconstruction with initial guess (b); (d) reconstruction in local domain.

Challenging Issues in X-ray CT: Removing Metal Artifact

Hyoung Suk Park

CT image from the metallic objects

- With the presence of metallic objects in the field of view, bright and dark streaking artifacts are introduced.
- It is still challenging issue due to serious difficulties in analyzing the X-ray data.
- Our goal is to provide a rigorous characterization of the metal streaking artifacts using the notion of the wavefront set.

Basic CT Reconstruction Algorithm

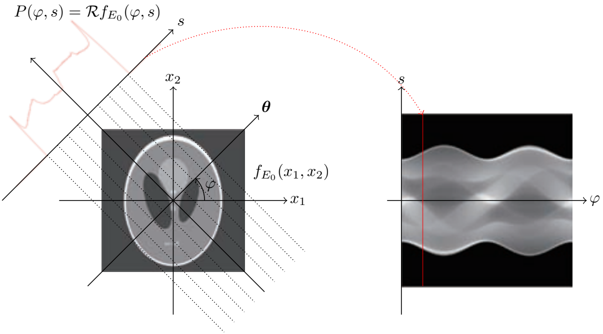

$$\mathcal{R}f_{E_0}(\varphi, s) = \int_{\mathbb{R}^2} f_{E_0}(\mathbf{x})\delta(\mathbf{x}\cdot\boldsymbol{\theta} - s)d\mathbf{x}$$: Radon transform

$$f_{E_0}(\mathbf{x}) = \frac{1}{4\pi}\mathcal{R}^*\mathcal{I}^{-1}\mathcal{R}f_{E_0}(\mathbf{x})$$: Inverse Radon transform

- X-ray has multiple energy levels. X-ray data and CT image are given by

(X-ray data) $$P(\varphi, s) = -\ln\left(\int_{\underline{E}}^{\overline{E}} \eta(E)\exp\{-\mathcal{R}f_E(\varphi, s)\}dE\right)$$

CT Reconstruction Error due to the Nonlinearity

- The difference between P and $\mathcal{R}f_{E_0}$ is represented by

$$[P - \mathcal{R}f_{E_0}](\varphi, s) \approx \int_{\underline{E}}^{\overline{E}} \eta(E') \int_{E_0}^{E'} \left[e^{-\mathcal{R}[f_E - f_{E_0}](\varphi,s)} \mathcal{R}\left[\frac{\partial f_E}{\partial E}\right](\varphi, s)\right] dEdE'$$

- These strong nonlinear effects lead to streaking artifacts.

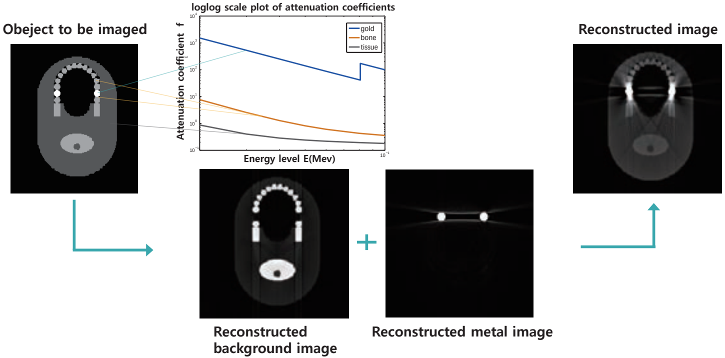

Mathematical Tool: Wavefront Set

- Wavefront Set: The wavefront set of f is given by

$$\mathrm{WF}(f) = \left\{(\mathbf{x}, \boldsymbol{\xi}) \in \mathbb{R}^2 \times (\mathbb{R}^2 \setminus \{\mathbf{0}\}) : \ \boldsymbol{\xi} \in \Sigma_{\mathbf{x}}(f)\right\},$$

-$\mathbf{x}$: Singularity (or jump in image)
-$\boldsymbol{\xi}$: Direction of singularity

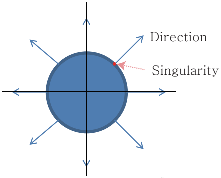

$$\mathrm{WF}(\chi_\Omega) = \left\{(\mathbf{x}, \boldsymbol{\xi}) \in \mathbb{R}^2 \times (\mathbb{R}^2 \setminus \{\mathbf{0}\}) : \mathbf{x} \in \partial\Omega, \ \boldsymbol{\xi} \text{ is the normal to } \partial\Omega \text{ at } \mathbf{x}\right\}.$$

Characterization of Streaking Artifacts I

- $L_{\varphi,s}$: streaking artifact $\Rightarrow \dim\left(\mathrm{Span}[\Sigma_{(\varphi,s)}(\mathcal{R}\chi_D)]\right) = 2$

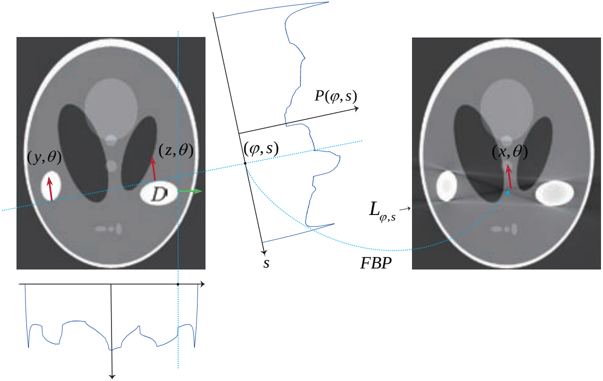

Meaning : If there exist distinct $\mathbf{x}_1, \mathbf{x}_2 \in \partial D$ such that the straight line $\mathbf{x}\cdot\boldsymbol{\theta} = s$ is tangent to ∂D at $\mathbf{x}_1$ and $\mathbf{x}_2$ simultaneously, then the streaking artifacts will occur on this straight line $\mathbf{x}\cdot\boldsymbol{\theta} = s$.

Characterization of Streaking Artifacts II

- D is strictly convex $\Rightarrow \mathrm{WF}(f_{\mathrm{CT}}) \subseteq \mathrm{WF}(f_{E_0})$

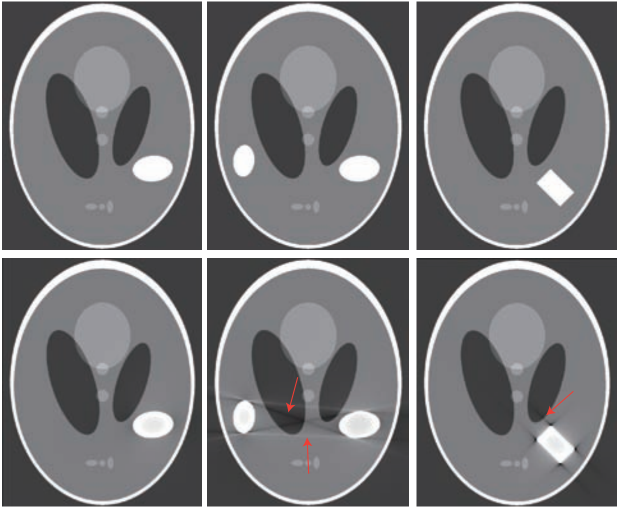

Other sources of Streaking Artifacts: Scattering and Noise

- Scattering effects: Assuming scattering to be a constant [Glover, 1982], we have

$$P(\varphi, s) = -\ln I(\varphi, s) = -\ln(\exp\{-\mathcal{R}f_{E_0}(\varphi, s)\} + c)$$

- Noise effects: Assuming that $N(\varphi, s) = \sum_{k=1}^{K} c_k \delta(\varphi - \varphi_k, s - s_k)$,

$$P(\varphi, s) = -\ln(\exp\{-\mathcal{R}f_{E_0}(\varphi, s)\} + N(\varphi, s))$$

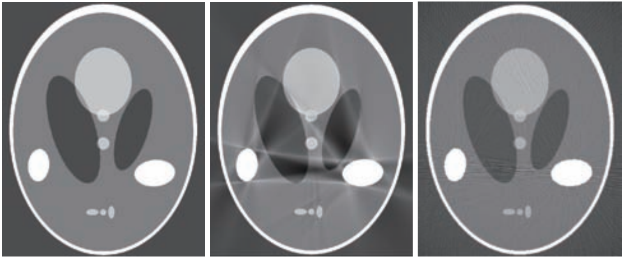

Original image Scattering Noise

Streaking Artifacts in CT Image

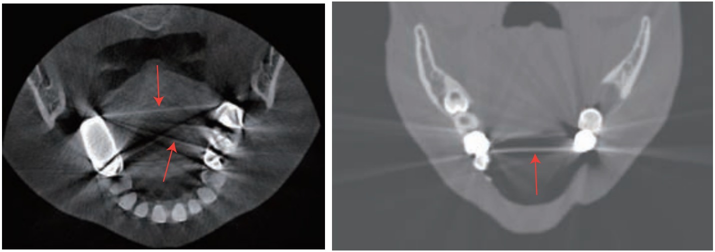

- Most streaking artifacts occur along the tangent line of boundary of metallic objects.
- Streaking artifacts can appear between metallic object and bone due to scattering or noise effect.

Remarks on Metal Artifacts Reduction Methods

- Goal: Try to find $P^\natural$ such that $P^\natural \in$ Range space $= \{\mathcal{R}f^\natural : f^\natural \in \mathcal{E}'\}$.
- Existing MAR methods: Inpainting based methods.

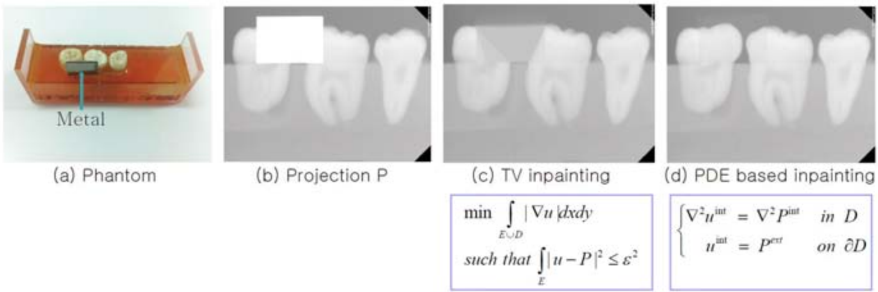

- TV inpainting may produce additional singularities due to the nature of total variation minimization.
- Based on the 1-1 correspondence, $\text{sing-supp}(f^\natural)$ corresponding to $\text{sing-supp}(P)$ in D can be recovered in reconstructed image.

Reconstructed CT Image Using MAR Methods

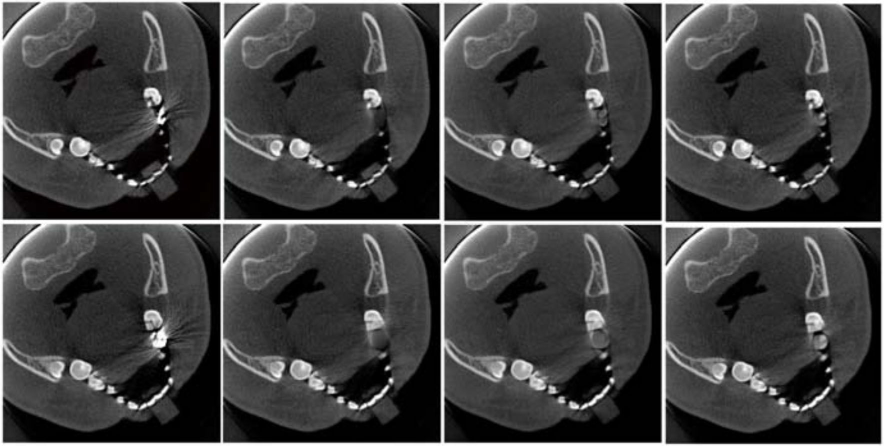

Reconstructed image | LI | TV inpainting | PDE based inpainting

Streaking artifacts are reduced in the reconstructed image, and bone information near the metallic objects is preserved, compared with LI and TV.

Remarks on Metal Artifacts Reduction Methods

- Metal image is recovered by solving the following minimization problem: (J.Choi *et al* 2011)

$$\min_{\mathbf{f}^{\natural}_{\mathrm{m}}} \ \|\mathbf{f}^{\natural}_{\mathrm{m}}\|_1 \ \text{ subject to } \|\mathbf{w} - \mathbf{L}\mathbf{f}^{\natural}_{\mathrm{m}}\|^2_{\mathbf{M}} \le \varepsilon,$$

\- $\mathbf{f}^{\natural}_{\mathrm{m}} := \mathbf{f}^{\natural} - \mathbf{f}^{\natural}_{\mathrm{b}}$ and $\mathbf{P} := \mathbf{u}^{\natural} + \mathbf{w}.$

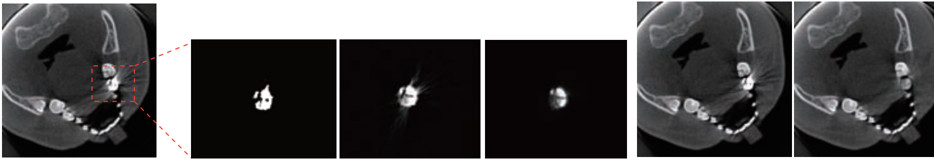

Uncorrected CT image | Simple thresholding | FDK algorithm | Corrected metal image | Uncorrected CT image | Background Image

MAR with controlling wave front set

- D is strictly convex $\Rightarrow$ No streaking artifacts

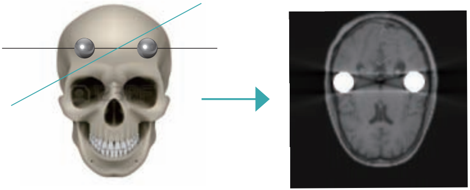

Reconstructed CT image

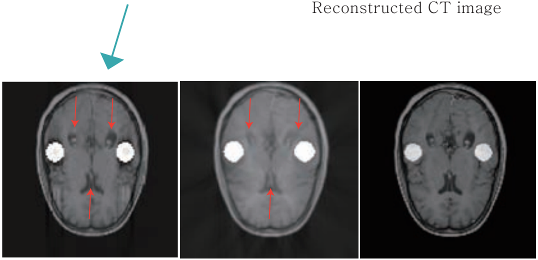

$\min_{\mathbf{f}^\natural} \|\mathbf{W}\nabla \mathbf{f}^\natural\|_1$ s.t $\|\mathbf{L}\mathbf{f}^\natural - \mathbf{P}\|_2^2 \leq \epsilon$

LI + thresholding

Original image

Blood Flow Velocity in LV using Ultrasound

Jaeseong Jang

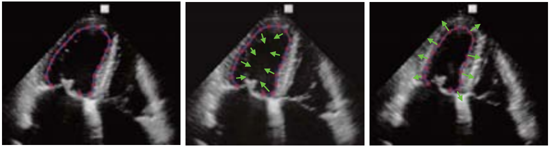

(a) (b) (c)

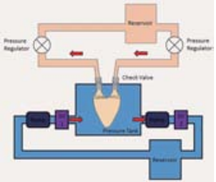

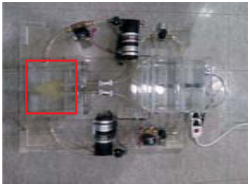

Introduction

Aim : **Visualization of blood flow velocity** in the Left Ventricle using

- Model which consider **3D fluid dynamics** on our 2D imaging plane,
- **Color Doppler data** which provides us **projected velocity information**.

(Amid)

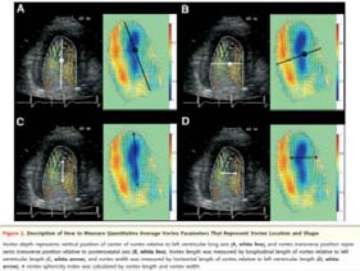

(Hong et al.)

- Some existing methods need to inject contrast agent to obtain particle images.

Color Doppler Data

- **Color Doppler data** provides **Projected velocity** component along the ultrasound beam direction.
- This measurement is **limited on the 2D imaging plane.**
- We combine the projected information with **Navier-Stokes equations.**

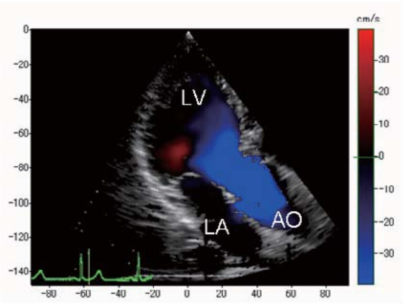

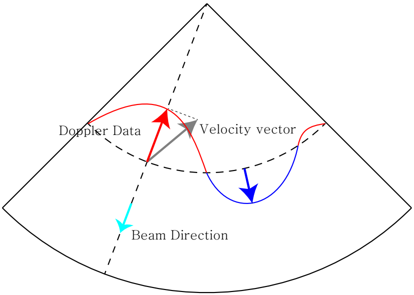

Modelling of Our 2D Model

- The blood flow is governed by 3D incompressible Navier-Stokes equation (NSE).
- Since we are interested in recovering (u, v), we rewrite 3D NSE as

$$
\begin{cases}
\dfrac{\partial u}{\partial t} + u\dfrac{\partial u}{\partial x} + v\dfrac{\partial u}{\partial y} = -\dfrac{1}{\rho}\dfrac{\partial p}{\partial x} + \dfrac{\mu}{\rho}\left(\dfrac{\partial^2 u}{\partial x^2} + \dfrac{\partial^2 u}{\partial y^2}\right) + f_1, \\
\dfrac{\partial v}{\partial t} + u\dfrac{\partial v}{\partial x} + v\dfrac{\partial v}{\partial y} = -\dfrac{1}{\rho}\dfrac{\partial p}{\partial y} + \dfrac{\mu}{\rho}\left(\dfrac{\partial^2 v}{\partial x^2} + \dfrac{\partial^2 v}{\partial y^2}\right) + f_2, \\
\dfrac{\partial u}{\partial x} + \dfrac{\partial v}{\partial y} = -\dfrac{\partial w}{\partial z}.
\end{cases}
$$

- We need **Additional terms** to 2D NSE and cannot use **2D incompressibility** for u and v.

2D Navier-Stokes equation with mass source

$$\begin{cases} \dfrac{\partial u}{\partial t} + u\dfrac{\partial u}{\partial x} + v\dfrac{\partial u}{\partial y} = -\dfrac{1}{\rho}\dfrac{\partial p}{\partial x} + \dfrac{\mu}{\rho}\nabla^2 u + \dfrac{\mu}{3\rho^2}\dfrac{\partial s}{\partial x}, \\ \dfrac{\partial v}{\partial t} + u\dfrac{\partial v}{\partial x} + v\dfrac{\partial v}{\partial y} = -\dfrac{1}{\rho}\dfrac{\partial p}{\partial y} + \dfrac{\mu}{\rho}\nabla^2 v + \dfrac{\mu}{3\rho^2}\dfrac{\partial s}{\partial y}, \\ \dfrac{\partial u}{\partial x} + \dfrac{\partial v}{\partial y} = \dfrac{s}{\rho}. \end{cases}$$

- u, v : x, y componenets of 2D velocity vector
- p : pressure
- s : mass source
- ρ, μ : fluid density and viscosity

Reconstruction Model

Combining the equation with Doppler data,

$$\begin{cases} \dfrac{\partial u}{\partial t} + u\dfrac{\partial u}{\partial x} + v\dfrac{\partial u}{\partial y} = -\dfrac{1}{\rho}\dfrac{\partial p}{\partial x} + \dfrac{\mu}{\rho}\nabla^2 u + \dfrac{\mu}{3\rho^2}\dfrac{\partial s}{\partial x}, \\ \dfrac{\partial v}{\partial t} + u\dfrac{\partial v}{\partial x} + v\dfrac{\partial v}{\partial y} = -\dfrac{1}{\rho}\dfrac{\partial p}{\partial y} + \dfrac{\mu}{\rho}\nabla^2 v + \dfrac{\mu}{3\rho^2}\dfrac{\partial s}{\partial y}, \\ \dfrac{\partial u}{\partial x} + \dfrac{\partial v}{\partial y} = \dfrac{s}{\rho} \quad \text{(Mass Source Term)}, \\ a_1 u + a_2 v = c \quad \text{(Color Doppler Data)}, \end{cases}$$

with boundary conditions for u, v, p, and s.

Simulation of LV Blood Flow

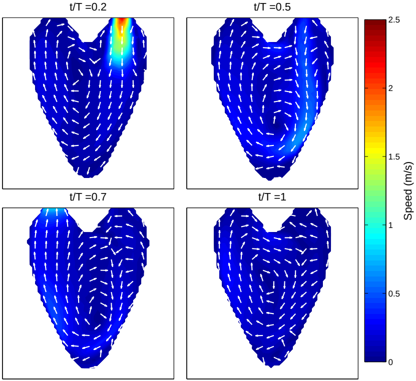

(a) Simulated velocity field

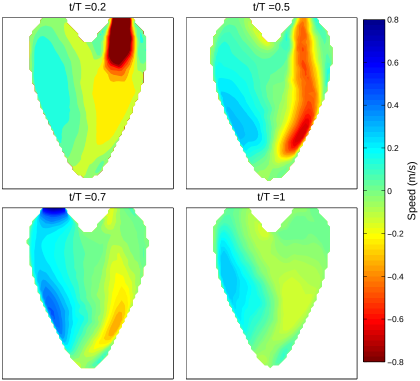

(b) Simulated color Doppler data

Figure: Simulation of LV blood flow

Reconstruction Results

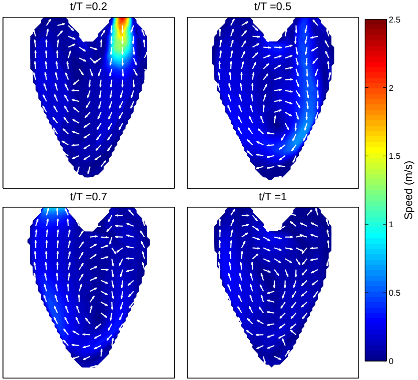

(a) Simulated velocity field

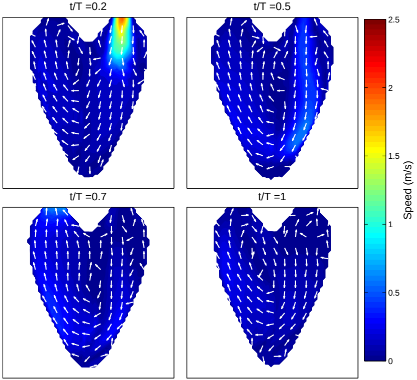

(b) Reconstructed velocity field

Thank you.

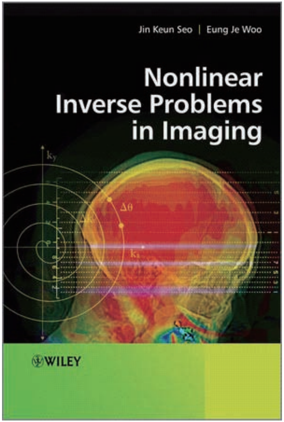

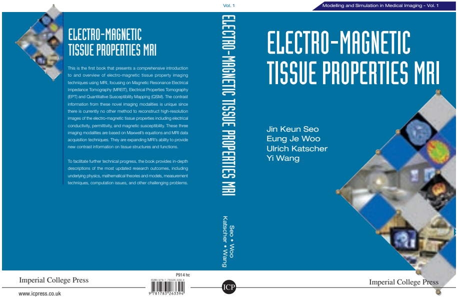

We focus on **experimental** mathematics. We develop mathematical theory in such a way that it can guide experiment on what to look for.

Modeling/Analysis⇔Numerical Simulation⇔Experiment